

**MODEL INDEPENDENT PARTICLE
ACCELERATOR CONTROL AND NONLINEAR
SPACE CHARGE COMPENSATION**

Alexander Scheinker

Submitted to the faculty of the University Graduate School
in partial fulfillment of the requirement
for the degree
Master of Science
in the Department of Physics,
Indiana University

December, 2013

Accepted by the Graduate Faculty, Indiana Univeristy, in partial fulfillment of the requirement for the degree of Master of Science.

Masters
Committee

Prof Shyh-Yuan Lee, Ph.D.

Prof. David V. Baxter, Ph.D.

Prof. Joshua C. Long, Ph.D.

December, 2013.

Copyright ©2013 by
Alexander Scheinker
ALL RIGHTS RESERVED

To Zina and Mama Pima.

Acknowledgments

Most of all, I would like to thank Dr. Shyh-Yuan Lee, I met professor Lee when I took my first US Particle Accelerator School (USPAS) course, his course, Accelerator Physics. Until then I had done some physics, some mathematics, and some engineering. In Professor Lee's course I was for the first time introduced to the rich field of accelerator physics, a wonderful, interesting combination, unification of those three subjects which I had previously studied as separate entities. Although I was at the time enrolled in a Ph.D. program, Professor Lee encouraged me to also enroll in the USPAS/Indiana University Masters in Accelerator Physics program. I am very grateful to Dr. Lee for his advice and encouragement, being part of the USPAS program has been very rewarding, I've had the opportunity to study many aspects of accelerator physics cities across the US, and have met many wonderful people, all involved in accelerator physics programs throughout the world. I would also like to thank Susan Winchester, she has been very encouraging of my enrollment in USPAS, and very helpful throughout the years. I am of course also thankful to my parents, Anna and Vladimir, for their never ending support and encouragement in everything that I try to do.

Abstract

Alexander Scheinker

Model Independent Particle Accelerator Control and Nonlinear Space Charge Compensation

This work can be broken down into two main parts, the first an analytic derivation for the averaged dynamics of a space-charge dominated beam, which is matched into a non-linear FODO lattice utilizing higher order magnetic poles and the second focused on model independent accelerator control and component tuning. Because real, non-idealized particle beams experience nonlinear space charge forces, it is impossible to match them to a lattice of linear magnetic components such as a pure quadrupole FODO setup. As was calculated by Batygin, the introduction of nonlinear focusing elements allows one to match a nonlinear space-charge dominated beam to a lattice, which may be adiabatically changed into a standard quadrupole FODO lattice, in such a way so that the beam itself becomes well matched to the linear lattice. The first part of this thesis calculates the averaged dynamics of a beam in such a nonlinear focusing lattice. Because particle accelerators are complex and beam dynamics are nonlinear, with time-varying dynamics of and coupling between many components, an adaptive, model-independent control or tuning scheme may be useful to replace or greatly shorten the duration of typical lengthy hand-tuning of components, tuning which must be re-done many times due to un-modeled behavior such as thermal cycling, arbitrary phase drift of RF systems, and beam source fluctuations.

Contents

Acceptance	ii
Acknowledgments	v
Abstract	vi
1 Introduction	1
2 Nonlinear Magnets to Compensate for Nonlinear Space Charge	2
2.1 Results	2
2.1.1 Overview	3
3 Background: Matching of a Nonuniform Space Charge Dominated Beam	4
3.0.2 Self-consistent space charge potential of the beam	4
3.0.3 Matching channel for charge dominated beam	6
3.1 Main Results	8
3.1.1 $\Delta = 0$	16
3.1.2 $\Delta = -\frac{L}{4}$	21
3.2 Simulation Results	21
3.3 Conclusions	22

4	Rotation Rate Adaptive Tuning	24
4.0.1	Physical Motivation	24
5	Control Theory Background	28
5.1	Lyapunov Functions and Stability Theory	28
5.1.1	Stability	28
5.1.2	Lyapunov Functions	30
5.2	Weak Convergence	33
6	General Adaptive Scheme	39
6.1	Adaptive Feedback for Simultaneous Multi-Parameter Optimization	39
6.1.1	Multi-Objective Optimization	42
6.2	Some Discussion on the RR Method	43
7	Guidelines for Digital Implementation	45
7.0.1	Cost and Constraints	45
7.0.2	Choice of ω , and Δ	46
7.0.3	Choice of k and α	47
7.0.4	Digital Resolution	47
7.0.5	Normalization of Parameters	48
8	Simulation Results	49
8.1	Tuning 22 Quadrupole Magnets and 2 Buncher Cavities	49
8.1.1	Magnet Tuning for Beam Transport	50
8.1.2	Magnet and RF Buncher Cavity Tuning	53
8.1.3	Adaptation to Time Varying Phase Delay and Beam Characteristics	56

List of Tables

List of Figures

- 3.1 Lines of equal values of the function $C = \frac{1}{2}r^2 + \zeta r^6 \cos(4\varphi) + \frac{\zeta^2}{2}r^4$, for $\zeta = -0.03$: (a) $C = 0.05$, (b) $C = 0.25$, (c) $C = 0.5$, and (d) $C = 0.82$ (left). Beam charge density distribution for (d) (right). 7
- 3.2 Two periodic sets of alternating magnets, in which the individual magnet lengths are given by D and the separation between magnets of the same kind is d , resulting in an overall, periodic structure with period $L = 2(D + d)$. The offset between two different types of magnets is Δ . 9
- 3.3 FODO quadrupole-duodecapole channel with combined lenses with $\Delta = 0$, period $L = 15\text{cm}$, lens length of $D = 5\text{cm}$, and adiabatic decline of duodecapole component to zero over a distance of 7 periods. 10
- 3.4 Comparison of emittance growth and halo formation (two left columns) and adiabatic matching (two right columns) of the 50 keV, 20 mA, 0.05 π cm mrad proton beam in FODO quadrupole channel with the period of $L = 15$ cm, lens length of $D = 5$ cm and field gradient of $G_2 = 1.325$ kV/cm² and adiabatic decline of duodecapole component from $G_6 = -0.005$ kV/cm⁶ to zero for the distance of 7 periods. Numbers indicate FODO periods. 23

4.1	The subfigure in the bottom left shows the rotation rate, $\frac{\partial \theta}{\partial t} = \omega + \frac{\partial C(x,y)}{\partial t}$, for the part of the trajectory that is bold red, which takes place during the first 0.5 seconds of simulation. The rotation of the parameters' velocity vector $\mathbf{v}(t)$ slows down when heading towards the minimum of $C(x, y) = x^2 + y^2$, at which time $k \frac{\partial C}{\partial t} < 0$, and speeds up when heading away from the minimum, when $k \frac{\partial C}{\partial t} > 0$. The system ends up spending more time heading towards and approaches the minimum of $C(x, y)$	27
5.1	Stable (a), asymptotically stable (b), and exponentially stable (c) equilibrium point $\mathbf{x} = 0$	30
6.1	Tuning of the i^{th} component p_i of $\mathbf{p} = (p_1, \dots, p_n) \in \mathbb{R}^n$. The symbol $\frac{1}{s}$ denotes the Laplace Transform of an integrator, so that in the above diagram $p_i(t) = p_i(0) + \int_0^t u_i(\tau) d\tau$	40
8.1	Simplified schematic of the LANSCE H^+ injector and transport region.	51
8.2	The surviving current at the end of the beam transport over 2500 iteration steps is shown for an initial beam current of 13mA.	51
8.3	Evolution of the magnet current settings to the magnets over 2500 iteration steps.	52
8.4	RMS beam size at the end of the iterative tuning scheme.	52
8.5	Magnet settings at the end of the iterative tuning scheme compared to 2011 tune up settings.	53
8.6	The surviving current at the end of the beam transport over 2000 iteration steps is shown for an initial beam current of 15mA.	54
8.7	New magnet settings after optimization.	55
8.8	Evolution of buncher cavity phase settings over 2000 iteration steps. .	55

8.9	Comparison of RMS beam size along the accelerator for the 2011 tune-based magnet settings and arbitrary phase (dashed) with RMS beam size following RR tune (solid).	56
8.10	Surviving beam current along the machine with 2011 tune-based magnet settings and arbitrary phase (red) and following RR tune (blue). . .	57
8.11	The input beam was gradually changed over 18000 time steps.	57
8.12	Evolution of the buncher phase settings, during, and after variation of beam and phase delay parameters.	58
8.13	Evolution of the magnet gradients before, during, and after variation of beam and phase delay parameters.	58
8.14	New magnet settings after optimization.	59
8.15	Comparison of RMS beam size along the accelerator for the 2011 tune-based magnet settings (dashed) and after the beam initial conditions have changed and RR tuning has re-focused and matched the beam (solid).	60
8.16	Surviving beam current at the end of the second DTL tank with and without adaptive RR tuning. The cost evolution during the tuning process is also shown.	61

Chapter 1

Introduction

The results of this thesis can be broken down into two main parts. Part I, Chapters 1 and 2 are concerned with an analytic derivation for the averaged dynamics of a space-charge dominated beam, which is matched into a non-linear FODO lattice utilizing higher order magnetic poles. The developed FODO lattice consists of a combination of quadrupole and duodecapole components, which matches a realistic beam, with non-linear space charge forces. As the duodecapole components are adiabatically reduced, the beam is finally matched into a standard, purely quadrupole FODO lattice. Part II, Chapters 3 - 8, are focused on a model-independent, adaptive control scheme for automated control and tuning of uncertain systems, such as particle accelerator magnet settings, despite unknown beam distribution, time varying system characteristics, such as those due to thermal cycling and beam source fluctuations.

Chapter 2

Nonlinear Magnets to Compensate for Nonlinear Space Charge

2.1 Results

Nonuniform space charge dominated beams cannot be perfectly matched with a linear focusing channel resulting in emittance growth and halo formation. It was shown by Y. Batygin [24] how to transport an intense, nonuniform beam without halo formation. In this work we present a practical structure for the implementation of the stabilizing fields as derived in [24]. The developed FODO lattice consists of a combination of quadrupole and duodecapole components, which matches a realistic beam, with non-linear space charge forces. As the duodecapole components are adiabatically reduced, the beam is finally matched into a standard, purely quadrupole FODO structure.

2.1.1 Overview

In Section 3 we give a brief review of the work by Batygin [24], in which the required field for transport of a nonuniform space charge dominated beam without halo growth was derived, having the form

$$\begin{aligned} \vec{E} = & \left[-\hat{r} (G_2 r \cos(2\varphi) + G_6 r^5 \cos(6\varphi)) \right. \\ & \left. + \hat{\varphi} (G_2 r \sin(2\varphi) + G_6 r^5 \sin(6\varphi)) \right] \sin(\omega_0 t), \end{aligned}$$

which would require a difficult to manufacture four vane quadrupole structure for implementation. In Section 3.1 we remove the $\sin(\omega_0 t)$ term by approximating it with a FODO structure. We show that on average our structure gives us the same FODO results as derived by Kapchinsky [25]. In Section 3.2 we demonstrate the stabilizing properties with a numerical simulation.

Chapter 3

Background: Matching of a Nonuniform Space Charge Dominated Beam

3.0.2 Self-consistent space charge potential of the beam

In [24] Batygin starts with a single-particle Hamiltonian in a focusing channel

$$K = c\sqrt{m^2c^2 + \|\vec{P} - q\vec{A}\|^2} + qU_{\text{ext}} + qU_b, \quad (3.1)$$

where $\vec{P} = (P_x, P_y, P_z)$ is a canonical momentum of particles; $\vec{A} = (A_x, A_y, A_z)$ is a vector potential, $U_{\text{ext}}(x, y)$ is a scalar potential of the focusing field, and $U_b(x, y)$ is a space charge potential of the beam. By considering the Lorentz transformation of a reference frame in which the particles are static, as well as making the assumption that the Alfvén current $I \ll \beta\gamma I_c$, where $I_c = 4\pi\epsilon_0 mc^3/q$ is the characteristic value of beam current, Batygin arrives at the simplified single-particle Hamiltonian:

$$H = \frac{p_x^2 + p_y^2}{2m\gamma} + qU_{\text{ext}} + q\frac{U_b}{\gamma^2}. \quad (3.2)$$

Background: Matching of a Nonuniform Space Charge Dominated Beam

Next, in order to find a self-consistent particle distribution the following variables are introduced:

$$V_{\text{ext}} = \frac{qU_{\text{ext}}}{H_0}, \quad V_b = \frac{qU_b}{H_0}, \quad \xi = \frac{r}{a}, \quad H_0 = \frac{mc^2}{4\gamma} \left(\frac{\epsilon}{R} \right)^2, \quad (3.3)$$

where a is the radius of the channel, R is the beam radius, and ϵ is $4 \times$ rms normalized beam emittance. The unknown potential V_b is then expressed as a Fourier-Bessel series,

$$V_b = V_0 + \bar{V}_b,$$

where

$$\bar{V}_b = \sum_{n=0}^{\infty} \sum_{m=1}^{\infty} J_n(\nu_{nm}\xi) (A_{nm} \cos(n\varphi) + B_{nm} \sin(n\varphi)), \quad (3.4)$$

where $J_n(x)$ is a Bessel function and ν_{nm} is the m th root of the equation $J_n(x) = 0$. The expansion (3.4) satisfies the Dirichlet boundary condition at the conductive surface of a round pipe $V_b(a) = V_0$. The constant V_0 is defined such that the total potential of the structure vanishes at the axis:

$$V_{\text{ext}}(0, \varphi) + \frac{\bar{V}_b(0, \varphi)}{\gamma^2} + \frac{V_0}{\gamma^2} = 0. \quad (3.5)$$

After making several approximations Batygin arrives at the simplified approximate form of Poisson's equation:

$$V_0 + (1 + \delta)\bar{V}_b = \gamma^2(1 - V_{\text{ext}}), \quad (3.6)$$

where

$$\delta = \frac{1}{bk} \ll 1,$$

$$b = \frac{2}{\beta\gamma} \frac{I}{\epsilon^2} \frac{R^2}{I_c},$$

is the dimensionless beam brightness,

$$I_c = \frac{4\pi\epsilon_0 mc^3}{q}$$

Background: Matching of a Nonuniform Space Charge Dominated Beam

is the characteristic value of beam current, and k is the average value of density

$$k = \frac{\rho_0}{\bar{\rho}}$$

for different particle distributions. The self-consistent space charge dominated beam potential near axis is then

$$V_b = -\frac{\gamma^2}{1+\delta} V_{\text{ext}} \quad (3.7)$$

and the electric field is given by $\vec{E} = -\text{grad } U$ as

$$\vec{E}_b = -\frac{\gamma^2}{1+\delta} \vec{E}_{\text{ext}}. \quad (3.8)$$

Equation (3.7) implies that a space charge dominated beam compensates for the focusing field in the beam core regardless of the applied external focusing potential, a phenomenon known as Debye shielding for nonneutral plasmas. The space charge distribution required for matching is then derived from Poisson's equation as

$$\rho_b = -\epsilon_0 \Delta U_b = \frac{\epsilon_0}{1+\delta} \gamma^2 \Delta U_{\text{ext}}. \quad (3.9)$$

3.0.3 Matching channel for charge dominated beam

In [24] a uniform four vane structure with potential

$$U(r, \varphi, t) = \left(\frac{G_2}{2} r^2 \cos(2\varphi) + \frac{G_6}{6} r^6 \cos(6\varphi) \right) \sin(\omega_0 t), \quad (3.10)$$

is considered, where G_2 is a quadrupole gradient, G_6 is a duodecapole component, and $\omega_0 = 2\pi c/\lambda$ is an operational frequency. Equipotential lines and required matched beam charge density distribution are shown in Figure 3.1. The electrical field of this structure is

$$\begin{aligned} \vec{E} = & \left[-\hat{r} (G_2 r \cos(2\varphi) + G_6 r^5 \cos(6\varphi)) \right. \\ & \left. + \hat{\varphi} (G_2 r \sin(2\varphi) + G_6 r^5 \sin(6\varphi)) \right] \sin(\omega_0 t), \end{aligned} \quad (3.11)$$

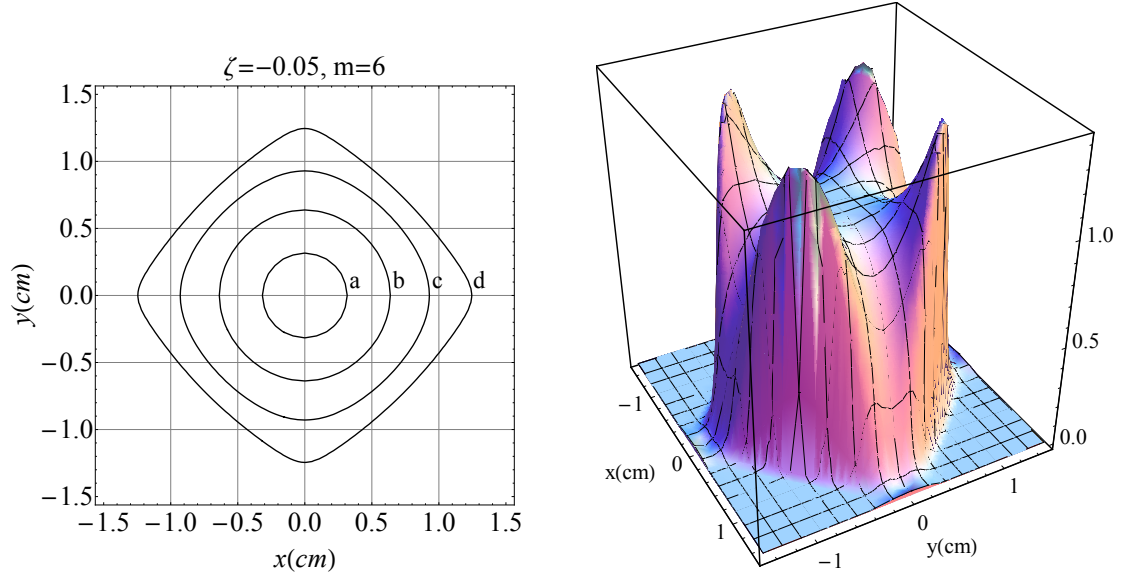


Figure 3.1: Lines of equal values of the function $C = \frac{1}{2}r^2 + \zeta r^6 \cos(4\varphi) + \frac{\zeta^2}{2}r^{10}$, for $\zeta = -0.03$: (a) $C = 0.05$, (b) $C = 0.25$, (c) $C = 0.5$, and (d) $C = 0.82$ (left). Beam charge density distribution for (d) (right).

which can be described by effective potential

$$U_{\text{ext}}(r, \varphi) = \frac{mc^2}{q} \frac{\mu_0^2}{\lambda^2} \left[\frac{1}{2}r^2 + \zeta r^6 \cos(4\varphi) + \frac{\zeta^2}{2}r^{10} \right], \quad (3.12)$$

where μ_0 is a smooth transverse oscillation and ζ is the ratio of field components:

$$\mu_0 = \frac{qG_2\lambda^2}{\sqrt{8\pi mc^2}\sqrt{\gamma}}, \quad \zeta = \frac{G_6}{G_2}. \quad (3.13)$$

By applying Eq.(3.9) an expression is found for a self consistent space charge distribution of the beam in the structure (3.12):

$$\begin{aligned} \rho_b &= \rho_0(1 + 10\zeta r^4 \cos(4\varphi) + 25\zeta^2 r^8), \\ \rho_0 &= \frac{2\gamma^2}{1 + \delta} \frac{mc^2}{q} \frac{\epsilon_0 \mu_0^2}{\lambda^2}. \end{aligned} \quad (3.14)$$

Integrating the space charge density over radius and azimuth angle $0 \leq r \leq R$, $0 \leq \varphi \leq 2\pi$ gives the total number of transported particles per unit length,

$$N = \frac{\pi\rho_0}{q}(R^2 + 5\zeta^2 R^10), \quad (3.15)$$

from which the space charge particle density at the beam center and parameter k are found to be

$$\begin{aligned} \rho_0 &= \frac{1}{1 + 5\zeta^2 R^8} \frac{I}{\beta c \pi R^2}, \\ k &= \frac{1}{1 + 5\zeta^2 R^8}. \end{aligned} \quad (3.16)$$

Finally comparing equations (3.14) and (3.16) the required value of the focusing gradient is found to be

$$G_2 = \sqrt{8\pi} \frac{mc^2}{qR\lambda} \sqrt{\frac{\epsilon^2}{R^2} + \frac{3I}{I_c\beta\gamma}}, \quad G_6 = -\frac{G_2}{12\beta\gamma R^4} \frac{I}{I_c} \left(\frac{\epsilon^2}{R^2} + \frac{3I}{I_c\beta\gamma} \right)^{-1}. \quad (3.17)$$

3.1 Main Results

The focusing field, (3.11), can be realized by a uniform four-vane structure with specific pole-tip shape imposing duodecapole component in pure quadrupole. The construction of such a structure is mechanically complicated and expensive. We present a simpler and more practical structure, as shown in Figure 3.3. We consider a FODO lattice of lenses with combined quadrupole $G_2(z)$ and duodecapole $G_6(z)$ magnetic field components. Such magnets can be done as a combination of conventional quadrupoles with current sheet magnets [29]. The quadrupole field is kept constant along the structure while duodecapole component gradually decreases from nominal value to zero at a certain distance. It gives us the possibility to match initially non-uniform beam with the non-linear focusing channel and adiabatically transform it to the beam matched with quadrupole focusing structure.

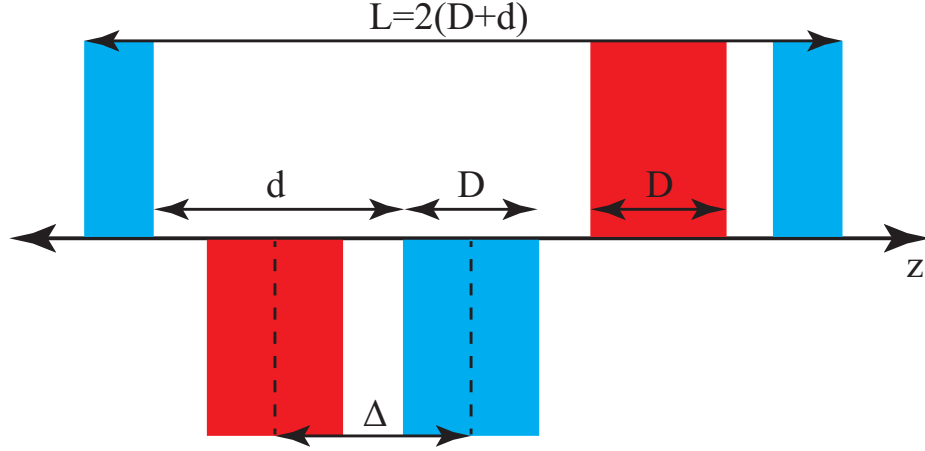


Figure 3.2: Two periodic sets of alternating magnets, in which the individual magnet lengths are given by D and the separation between magnets of the same kind is d , resulting in an overall, periodic structure with period $L = 2(D + d)$. The offset between two different types of magnets is Δ .

In what follows, for notational simplicity, we describe dynamics in terms of an electrical transverse field FODO structure. The average dynamics derived in this way can be equivalently achieved by replaced electric poles with properly rotated magnetic poles throughout, with an additional multiplicative factor depending on the fixed beam velocity. The required electric field is:

$$\vec{E} = [-\hat{r} (G_2 r \sin(2\varphi) + G_6 r^5 \sin(6\varphi)) + \hat{\varphi} (G_2 r \cos(2\varphi) + G_6 r^5 \cos(6\varphi))] \sin(\omega_0 t) \quad (3.18)$$

and can be realized by a uniform four vane structure. The construction of such a structure is mechanically complicated and expensive, requiring precision similar to that of constructing a RFQ. We present a much simpler and more practical structure, whose field, on average matches that of (3.18). Consider two FODO lattices, one of

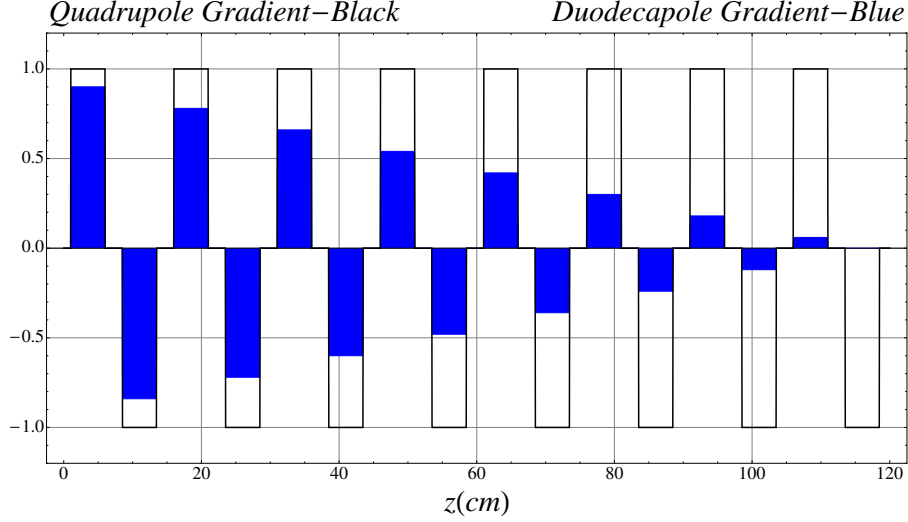


Figure 3.3: FODO quadrupole-duodecapole channel with combined lenses with $\Delta = 0$, period $L = 15\text{cm}$, lens length of $D = 5\text{cm}$, and adiabatic decline of duodecapole component to zero over a distance of 7 periods.

quadrupole and the other of duodecapole components, each with gaps of length d , field regions of length D , offset from each other by a length of Δ . The total unit length is then given by $L = 2(D + d)$ and the arrangement is as in Figure 3.2. The field equation is

$$\begin{aligned} \vec{E} = & -\hat{r} (G_Q(z)G_2r \sin(2\varphi) + G_D(z)G_6r^5 \sin(6\varphi)) \\ & +\hat{\varphi} (G_Q(z)G_2r \cos(2\varphi) + G_D(z)G_6r^5 \cos(6\varphi)), \end{aligned}$$

which we write as

$$\vec{E} = \vec{G}_D(r, \varphi)G_D(z) + \vec{G}_Q(r, \varphi)G_Q(z),$$

where

$$\begin{aligned}\vec{G}_Q(r, \varphi) &= -\hat{r}G_2r \cos(2\varphi) + \hat{\varphi}G_2r \sin(2\varphi) \\ \vec{G}_D(r, \varphi) &= -\hat{r}G_6r^5 \cos(6\varphi) + \hat{\varphi}G_6r^5 \sin(6\varphi) \\ G_Q(z) &= \begin{cases} 1 : & z \leq \frac{D}{2} \\ 0 : & \frac{D}{2} \leq z \leq d + \frac{D}{2} \\ -1 : & d + \frac{D}{2} \leq z \leq d + \frac{3D}{2} \\ 0 : & d + \frac{3D}{2} \leq z \leq 2d + \frac{3D}{2} \\ & \vdots \end{cases} , \\ G_D(z) &= G_Q(z - \Delta).\end{aligned}$$

This structure is chosen so that its time dependence, from the point of view of a beam traveling at high velocity is approximately $\sin(\omega_0 t)$. In order to perform analysis we represent these periodic lattices with their Fourier Series.

Given

$$a_n = \frac{1}{L} \left[\int_0^{2L} G_Q(z) \cos\left(\frac{n\pi z}{L}\right) dz \right], \quad (3.19)$$

we rewrite the end point of the integral as $2L = 4(D + d)$ and expand

$$\begin{aligned}a_n &= \frac{1}{L} \int_0^{\frac{D}{2}} \cos\left(\frac{n\pi z}{L}\right) dz - \frac{1}{L} \int_{d+\frac{D}{2}}^{d+\frac{3D}{2}} \cos\left(\frac{n\pi z}{L}\right) dz \\ &+ \frac{1}{L} \int_{2d+\frac{3D}{2}}^{2d+\frac{5D}{2}} \cos\left(\frac{n\pi z}{L}\right) dz - \frac{1}{L} \int_{3d+\frac{5D}{2}}^{3d+\frac{7D}{2}} \cos\left(\frac{n\pi z}{L}\right) dz \\ &+ \frac{1}{L} \int_{4d+\frac{7D}{2}}^{4d+4D} \cos\left(\frac{n\pi z}{L}\right) dz.\end{aligned} \quad (3.20)$$

Evaluating the integrals in (3.20) we get

$$\begin{aligned}
a_n = & \frac{1}{n\pi} \sin\left(\frac{n\pi D}{2L}\right) \\
& - \frac{1}{n\pi} \left[\sin\left(\frac{n\pi}{2} + \frac{n\pi D}{2L}\right) - \sin\left(\frac{n\pi}{2} - \frac{n\pi D}{2L}\right) \right] \\
& + \frac{1}{n\pi} \left[\sin\left(n\pi + \frac{n\pi D}{2L}\right) - \sin\left(n\pi - \frac{n\pi D}{2L}\right) \right] \\
& + \frac{1}{n\pi} \left[-\sin\left(\frac{3n\pi}{2} + \frac{n\pi D}{2L}\right) + \sin\left(\frac{3n\pi}{2} - \frac{n\pi D}{2L}\right) \right] \\
& - \frac{1}{n\pi} \left[\sin\left(2n\pi - \frac{n\pi D}{2L}\right) \right].
\end{aligned} \tag{3.21}$$

We expand the terms in (3.21) using the trigonometric identities

$$\sin(a+b) = \sin(a)\cos(b) + \cos(a)\sin(b)$$

$$\sin(a-b) = \sin(a)\cos(b) - \cos(a)\sin(b)$$

and after cancellations get

$$a_n = \frac{1}{n\pi} \sin\left(\frac{n\pi D}{2L}\right) c_n, \tag{3.22}$$

where

$$c_n = 8, \text{ for } n \in \{2, 6, 10, 14, \dots\} = \{4j - 2, j \in \mathbb{N}\}, \tag{3.23}$$

and $c_n = 0$ for all other values of n .

Therefore, we get the Fourier coefficients

$$a_n = \frac{1}{L} \left[\int_0^{2L} G_Q(z) \cos\left(\frac{n\pi z}{L}\right) dz \right] = \frac{1}{n\pi} \sin\left(\frac{n\pi D}{2L}\right) c_n, \tag{3.24}$$

where

$$c_n = 8, \text{ for } n \in \{2, 6, 10, 14, \dots\} = \{4j - 2, j \in \mathbb{N}\},$$

$$c_n = 0, \text{ otherwise.} \tag{3.25}$$

Therefore

$$\vec{G}_Q(z, r, \varphi) = \vec{G}_Q(r, \varphi) \sum_{n=1}^{\infty} a_n \cos\left(\frac{n\pi z}{L}\right). \quad (3.26)$$

The duodecapole component of the field has the same Fourier Series as the Quadrupole component, shifted by $-\Delta$, therefore $\vec{G}_D(z, r, \varphi) = \vec{G}_Q(z - \Delta, r, \varphi)$,

$$\begin{aligned} \vec{G}_D(z, r, \varphi) = & \vec{G}_D(r, \varphi) \sum_{n=1}^{\infty} a_{n1}(\Delta) \cos\left(\frac{n\pi z}{L}\right) \\ & + \vec{G}_D(r, \varphi) \sum_{n=1}^{\infty} a_{n2}(\Delta) \sin\left(\frac{n\pi z}{L}\right), \end{aligned}$$

where

$$a_{n1}(\Delta) = a_n \cos\left(\frac{n\pi\Delta}{L}\right), \quad a_{n2}(\Delta) = a_n \sin\left(\frac{n\pi\Delta}{L}\right). \quad (3.27)$$

With $z = vt = \beta ct$ and $\omega = \frac{\beta c\pi}{L}$ the traveling particle's dynamics obey

$$\begin{aligned} m\ddot{r} = & q\vec{G}_Q(r, \varphi) \sum_{n=1}^{\infty} a_n \cos(n\omega t) + q\vec{G}_D(r, \varphi) \sum_{n=1}^{\infty} a_{n1}(\Delta) \cos(n\omega t) \\ & + q\vec{G}_D(r, \varphi) \sum_{n=1}^{\infty} a_{n2}(\Delta) \sin(n\omega t). \end{aligned} \quad (3.28)$$

We would like to calculate an effective potential for this particle's motion which will be the combination of a large, slowly oscillating term which we shall label as $R(t)$ and small quickly oscillating terms which we shall group together as $\zeta(t)$.

$$r(t) = R(t) + \zeta(t), \quad R \gg \zeta, \quad \ddot{R} \ll \ddot{\zeta}. \quad (3.29)$$

We take the first Taylor series terms of \vec{G}_Q and \vec{G}_D about R

$$\vec{G}_Q(R) \approx \vec{G}_Q(R) + \zeta \vec{\nabla} \cdot \vec{G}_Q(R) \quad (3.30)$$

$$\vec{G}_D(R) \approx \vec{G}_D(R) + \zeta \vec{\nabla} \cdot \vec{G}_D(R). \quad (3.31)$$

We now rewrite the dynamics equation (3.28) with (3.29) and the Taylor approximations, representing $\ddot{r} = \ddot{R}(t) + \ddot{\zeta}(t)$ as:

$$\begin{aligned}
\ddot{r} = & \frac{q}{m} \left[\vec{G}_Q(R) + \zeta \vec{\nabla} \cdot \vec{G}_Q(R) \right] \sum_{n=1}^{\infty} a_n \cos(n\omega t) \\
& + \frac{q}{m} \left[\vec{G}_D(R) + \zeta \vec{\nabla} \cdot \vec{G}_D(R) \right] \sum_{n=1}^{\infty} a_{n1}(\Delta) \cos(n\omega t) \\
& + \frac{q}{m} \left[\vec{G}_D(R) + \zeta \vec{\nabla} \cdot \vec{G}_D(R) \right] \sum_{n=1}^{\infty} a_{n2}(\Delta) \sin(n\omega t). \tag{3.32}
\end{aligned}$$

Now we take into account that $R \gg \zeta$ and $\ddot{R} \ll \ddot{\zeta}$ and so we rewrite the dynamics as

$$\begin{aligned}
\ddot{\zeta}(t) = & \frac{q}{m} \vec{G}_Q(R) \sum_{n=1}^{\infty} a_n \cos(n\omega t) \\
& + \frac{q}{m} \vec{G}_D(R) \sum_{n=1}^{\infty} a_{n1}(\Delta) \cos(n\omega t), \\
& + \frac{q}{m} \vec{G}_D(R) \sum_{n=1}^{\infty} a_{n2}(\Delta) \sin(n\omega t), \tag{3.33}
\end{aligned}$$

which we can solve explicitly, giving us

$$\begin{aligned}
\zeta(t) = & -\frac{q}{m\omega^2} \vec{G}_Q(R) \sum_{n=1}^{\infty} \frac{a_n}{n^2} \cos(n\omega t) \\
& -\frac{q}{m\omega^2} \vec{G}_D(R) \sum_{n=1}^{\infty} \frac{a_{n1}(\Delta)}{n^2} \cos(n\omega t) \\
& -\frac{q}{m\omega^2} \vec{G}_D(R) \sum_{n=1}^{\infty} \frac{a_{n2}(\Delta)}{n^2} \sin(n\omega t). \tag{3.34}
\end{aligned}$$

We now plug this solution, (3.34), into (3.32) and we expand \ddot{r} as:

$$\begin{aligned}
\ddot{r} = & \frac{q}{m} \sum_{n=1}^{\infty} \left[\vec{G}_Q(R) a_n \cos(n\omega t) + \vec{G}_D(R) a_{n1}(\Delta) \cos(n\omega t) + \vec{G}_D(R) a_{n2}(\Delta) \sin(n\omega t) \right] \\
& - \frac{q^2}{m^2 \omega^2} \sum_{n=1}^{\infty} G(n, m),
\end{aligned}$$

where $G(n, m)$ is given by the sum of the terms:

$$\begin{aligned}
& \vec{G}_Q(R) \frac{a_n}{n^2} \cos(n\omega t) \vec{\nabla} \cdot \vec{G}_Q(R) \sum_{m=1}^{\infty} a_m \cos(m\omega t) \\
& \vec{G}_Q(R) \frac{a_n}{n^2} \cos(n\omega t) \vec{\nabla} \cdot \vec{G}_D(R) \sum_{m=1}^{\infty} a_{m1}(\Delta) \cos(m\omega t) \\
& \vec{G}_Q(R) \frac{a_n}{n^2} \cos(n\omega t) \vec{\nabla} \cdot \vec{G}_D(R) \sum_{m=1}^{\infty} a_{m2}(\Delta) \sin(m\omega t) \\
& \vec{G}_D(R) \frac{a_{n1}(\Delta)}{n^2} \cos(n\omega t) \vec{\nabla} \cdot \vec{G}_Q(R) \sum_{m=1}^{\infty} a_m \cos(m\omega t) \\
& \vec{G}_D(R) \frac{a_{n1}(\Delta)}{n^2} \cos(n\omega t) \vec{\nabla} \cdot \vec{G}_D(R) \sum_{m=1}^{\infty} a_{m1}(\Delta) \cos(m\omega t) \\
& \vec{G}_D(R) \frac{a_{n1}(\Delta)}{n^2} \cos(n\omega t) \vec{\nabla} \cdot \vec{G}_D(R) \sum_{m=1}^{\infty} a_{m2}(\Delta) \sin(m\omega t) \\
& \vec{G}_D(R) \frac{a_{n2}(\Delta)}{n^2} \sin(n\omega t) \vec{\nabla} \cdot \vec{G}_Q(R) \sum_{m=1}^{\infty} a_m \cos(m\omega t) \\
& \vec{G}_D(R) \frac{a_{n2}(\Delta)}{n^2} \sin(n\omega t) \vec{\nabla} \cdot \vec{G}_D(R) \sum_{m=1}^{\infty} a_{m1}(\Delta) \cos(m\omega t) \\
& \vec{G}_D(R) \frac{a_{n2}(\Delta)}{n^2} \sin(n\omega t) \vec{\nabla} \cdot \vec{G}_D(R) \sum_{m=1}^{\infty} a_{m2}(\Delta) \sin(m\omega t).
\end{aligned}$$

To analyze this system further we apply averaging. All of the time-dependent functions have a common period of $T = \frac{2\pi}{\omega}$ and so we replace this system with a system averaged over the window T

$$\bar{g} = \frac{1}{T} \int_0^T g(t) dt. \quad (3.35)$$

Notice that because $\zeta(t)$ is a highly oscillating term it will average to zero. Also any products of the form $\cos(n\omega t) \cos(m\omega t)$ or $\sin(n\omega t) \sin(m\omega t)$ where $m \neq n$ average to zero as well as any products of the form $\cos(n\omega t) \sin(m\omega t)$ for all values of m and

n . And so we are left with

$$\begin{aligned}
\ddot{r} = & -\frac{q^2}{2m^2\omega^2} \sum_{n=1}^{\infty} \left[\vec{G}_Q(R) \vec{\nabla} \cdot \vec{G}_Q(R) \frac{a_n^2}{n^2} \right. \\
& + \vec{G}_Q(R) \vec{\nabla} \cdot \vec{G}_D(R) \frac{a_n a_{n1}(\Delta)}{n^2} \\
& + \vec{G}_D(R) \vec{\nabla} \cdot \vec{G}_Q(R) \frac{a_n a_{n1}(\Delta)}{n^2} \\
& + \vec{G}_D(R) \vec{\nabla} \cdot \vec{G}_D(R) \frac{a_{n1}^2(\Delta)}{n^2} \\
& \left. + \vec{G}_D(R) \vec{\nabla} \cdot \vec{G}_D(R) \frac{a_{n2}^2(\Delta)}{n^2} \right]. \tag{3.36}
\end{aligned}$$

We now consider what happens for different choices of Δ .

3.1.1 $\Delta = 0$

If $\Delta = 0$, then going back to the definitions (3.27) we see that $a_{n1}(0) = a_n$ and $a_{n2}(0) = 0$, and we can rewrite (3.36) as

$$\begin{aligned}
\ddot{r} = & -\frac{q^2}{2m^2\omega^2} \left[\vec{G}_Q(R) \vec{\nabla} \cdot \vec{G}_Q(R) + \vec{G}_Q(R) \vec{\nabla} \cdot \vec{G}_D(R) \right. \\
& \left. + \vec{G}_D(R) \vec{\nabla} \cdot \vec{G}_Q(R) + \vec{G}_D(R) \vec{\nabla} \cdot \vec{G}_D(R) \right] \sum_{n=1}^{\infty} \frac{a_n^2}{n^2}.
\end{aligned}$$

We now consider the summation term in more detail, recalling (3.25) we notice that all non-zero a_n are of the form

$$a_{4k-2}^2 = \left(\frac{8}{(4k-2)\pi} \right)^2 \sin^2 \left(\frac{(4k-2)\pi D}{2L} \right), \quad k \in \mathbb{N}$$

and write $\sum_{n=1}^{\infty} \left(\frac{a_n}{n} \right)^2$ as

$$\sum_{k=1}^{\infty} \frac{1}{(4k-2)^2} \left(\frac{8}{(4k-2)\pi} \right)^2 \sin^2 \left(\frac{(4k-2)\pi D}{2L} \right) = \frac{4}{\pi^2} \sum_{k=1}^{\infty} \frac{\sin^2 \left(\frac{(4k-2)\pi D}{2L} \right)}{(2k-1)^4}. \tag{3.37}$$

We consider the case where $L > D$, such that $0 < \frac{D}{L} < \frac{1}{2}$, we define $s = \frac{D}{L}$ and rewrite (3.37) as

$$\frac{4}{\pi^2} \sum_{k=1}^{\infty} \frac{\sin^2\left(\frac{(4k-2)\pi s}{2}\right)}{(2k-1)^4} = \frac{4}{\pi^2} \sum_{k=1}^{\infty} \frac{1 - \cos([4k-2]\pi s)}{2(2k-1)^4}. \quad (3.38)$$

Changing variables to $r = \pi s$ we get

$$\begin{aligned} & \frac{4}{\pi^2} \sum_{k=1}^{\infty} \frac{1 - \cos([4k-2]r)}{2(2k-1)^4} \\ &= \frac{4}{\pi^2} \sum_{k=1}^{\infty} \frac{1}{2(2k-1)^4} - \frac{4}{\pi^2} \sum_{k=1}^{\infty} \frac{\cos([4k-2]r)}{2(2k-1)^4} \\ &= \frac{4}{\pi^2} \frac{\pi^4}{96} - \frac{4}{\pi^2} \sum_{k=1}^{\infty} \frac{\cos([4k-2]r)}{(2k-1)^4} \\ &= \frac{4\pi^2}{96} - \frac{4}{\pi^2} \sum_{k=1}^{\infty} \frac{\cos([4k-2]r)}{(2k-1)^4} \\ &= \frac{4\pi^2}{96} - \frac{4}{\pi^2} 16 \sum_{k=1}^{\infty} \frac{\cos([4k-2]r)}{(4k-2)^4}. \end{aligned} \quad (3.39)$$

We now manipulate the sum (3.39) by repeatedly rewriting sine as the integral of cosine and vice versa, until it takes a form that we can recognize.

$$\begin{aligned} & 16 \sum_{k=1}^{\infty} \frac{\cos([4k-2]r)}{(4k-2)^4} \\ &= 16 \sum_{k=1}^{\infty} \left[\int_0^r \frac{-\sin([4k-2]s)}{(4k-2)^3} ds + \frac{1}{(4k-2)^4} \right] \\ &= 16 \sum_{k=1}^{\infty} \int_0^r \frac{-\sin([4k-2]s)}{(4k-2)^3} ds + 16 \sum_{k=1}^{\infty} \frac{1}{(4k-2)^4} \\ &= 16 \sum_{k=1}^{\infty} \int_0^r \frac{-\sin([4k-2]s)}{(4k-2)^3} ds + 16 \frac{\pi^4}{16 \times 96} \\ &= 16 \sum_{k=1}^{\infty} \int_0^r \frac{-\sin([4k-2]s)}{(4k-2)^3} ds + \frac{\pi^4}{96}. \end{aligned} \quad (3.40)$$

Continuing in the same way we get

$$\begin{aligned}
& 16 \sum_{k=1}^{\infty} \left[\int_0^r \frac{-\sin([4k-2]s)}{(4k-2)^3} ds \right] \\
&= 16 \sum_{k=1}^{\infty} \left[\int_0^r \left(\int_0^s \frac{-\cos([4k-2]w)}{(4k-2)^2} dw \right) ds \right]. \tag{3.41}
\end{aligned}$$

Taking one more integral we rewrite (3.41) as

$$\begin{aligned}
& 16 \sum_{k=1}^{\infty} \int_0^r \left(\int_0^s \left(\int_0^w \frac{\sin([4k-2]t)}{(4k-2)} dt \right) dw \right) ds \\
& - 16 \sum_{k=1}^{\infty} \int_0^r \left(\int_0^s \left(\frac{1}{(4k-2)^2} \right) dw \right) ds \\
&= 16 \sum_{k=1}^{\infty} \int_0^r \left(\int_0^s \left(\int_0^w \frac{\sin([4k-2]t)}{(4k-2)} dt \right) dw \right) ds \\
& - 16 \sum_{k=1}^{\infty} \int_0^r \left(\frac{s}{(4k-2)^2} \right) ds \\
&= 16 \sum_{k=1}^{\infty} \int_0^r \left(\int_0^s \left(\int_0^w \frac{\sin([4k-2]t)}{(4k-2)} dt \right) dw \right) ds \\
& - 16 \sum_{k=1}^{\infty} \frac{r^2}{2(4k-2)^2} \\
&= 16 \sum_{k=1}^{\infty} \int_0^r \left(\int_0^s \left(\int_0^w \frac{\sin([4k-2]t)}{(4k-2)} dt \right) dw \right) ds \\
& - 16 \frac{r^2}{2} \sum_{k=1}^{\infty} \frac{1}{(4k-2)^2} \\
&= 16 \sum_{k=1}^{\infty} \int_0^r \left(\int_0^s \left(\int_0^w \frac{\sin([4k-2]t)}{(4k-2)} dt \right) dw \right) ds \\
& - 8r^2 \frac{\pi^2}{32} \\
&= 16 \sum_{k=1}^{\infty} \int_0^r \left(\int_0^s \left(\int_0^w \frac{\sin([4k-2]t)}{(4k-2)} dt \right) dw \right) ds \\
& - \frac{r^2 \pi^2}{4}.
\end{aligned}$$

Finally we consider the term

$$\begin{aligned} & 16 \sum_{k=1}^{\infty} \int_0^r \left(\int_0^s \left(\int_0^w \frac{\sin([4k-2]t)}{(4k-2)} dt \right) dw \right) ds \\ &= 8 \sum_{k=1}^{\infty} \int_0^r \left(\int_0^s \left(\int_0^w \frac{\sin([4k-2]t)}{(2k-1)} dt \right) dw \right) ds. \end{aligned} \quad (3.42)$$

We now exchange the order of integration and summation and rewrite (3.42) as

$$8 \int_0^r \left(\int_0^s \left(\int_0^w \left[\sum_{k=1}^{\infty} \frac{\sin([4k-2]t)}{(2k-1)} \right] dt \right) dw \right) ds. \quad (3.43)$$

Recalling that the square function of period π , has the formula:

$$\text{square}_{\text{wave}}(t) = \frac{4}{\pi} \sum_{k=1}^{\infty} \frac{\sin([4k-2]t)}{(2k-1)} \quad (3.44)$$

we recognize that the sum in our equation is of the form

$$\frac{\pi}{4} \text{square}_{\text{wave}}(t) \quad (3.45)$$

and since we are considering the range $0 < t < \frac{\pi}{2}$, $\text{square}_{\text{wave}}(t) \equiv 1$ over our region of integration and so we have

$$\begin{aligned} & 8 \frac{\pi}{4} \int_0^r \left(\int_0^s \left(\int_0^w dt \right) dw \right) ds = 2\pi \int_0^r \left(\int_0^s w dw \right) ds \\ &= 2\pi \int_0^r \left(\frac{s^2}{2} \right) ds = 2\pi \frac{r^3}{6} = \frac{r^3 \pi}{3}. \end{aligned} \quad (3.46)$$

We have shown that, with our change of variables $s = \frac{D}{L}$ and $r = \pi s$

$$\begin{aligned}
\sum_{n=1}^{\infty} \left(\frac{a_n}{n} \right)^2 &= \frac{4\pi^2}{96} - \frac{4}{\pi^2} 16 \sum_{k=1}^{\infty} \frac{\cos([4k-2]r)}{(4k-2)^4} \\
&= \frac{4\pi^2}{96} - \frac{4}{\pi^2} \left[\frac{\pi^4}{96} - \frac{r^2\pi^2}{4} + \frac{r^3\pi}{3} \right] \\
&= \frac{4\pi^2}{96} - \frac{4\pi^2}{96} + r^2 - \frac{4r^3}{3\pi} \\
&= r^2 - \frac{4r^3}{3\pi} = \pi^2 s^2 - \frac{4\pi^3 s^3}{3\pi} \\
&= \frac{\pi^2 D^2}{L^2} - \frac{4\pi^2 D^3}{3L^3} \\
&= \frac{\pi^2 D^2}{L^2} \left[1 - \frac{4D}{3L} \right]. \tag{3.47}
\end{aligned}$$

Therefore, finally, (3.37) has simplified to

$$\frac{\pi^2 D^2}{L^2} \left(1 - \frac{4D}{3L} \right), \tag{3.48}$$

therefore we get

$$\ddot{r} = -\frac{q^2}{4m^2\omega^2} \frac{\pi^2 D^2}{L^2} \left(1 - \frac{4D}{3L} \right) \nabla \left(\vec{G}_Q + \vec{G}_D \right)^2, \tag{3.49}$$

which we rewrite as

$$\ddot{R} = -\frac{\mu_0^2}{L^2\gamma^2} \nabla \left(\vec{G}_Q + \vec{G}_D \right)^2, \tag{3.50}$$

where the term

$$\mu_0 = \left(\frac{qG_m}{\gamma m\beta c} \right) \left(\frac{LD}{2} \right) \sqrt{1 - \frac{4D}{3L}} \tag{3.51}$$

matches up exactly with the result calculated by Kapchinsky for a FODO lens system [25]. Therefore the beam's dynamics are described by the effective potential

$$U_{\text{eff}}(r, \varphi) = \frac{\mu_0^2}{L^2\gamma^2} \left(G_2^2 r^2 + 2G_2 G_6 r^6 \cos(6\varphi) + G_6^2 r^{10} \right). \tag{3.52}$$

The potential (3.52) matches exactly the desired effective potential (3.12) as analytically derived in [24].

3.1.2 $\Delta = -\frac{L}{4}$

If $\Delta = -\frac{L}{4}$, then going back to the definitions (3.27) we see that for all non-zero a_n , $a_{n1}^2(-\frac{L}{4}) = 0$ and $a_{n2}^2(-\frac{L}{4}) = a_n$, and therefore we can rewrite (3.36) as

$$\ddot{\vec{r}} = -\frac{q^2}{2m^2\omega^2} \left[\vec{G}_Q \nabla \cdot \vec{G}_Q + \vec{G}_D \nabla \cdot \vec{G}_D \right] \sum_{n=1}^{\infty} \left(\frac{a_n}{n} \right)^2, \quad (3.53)$$

which we simplify to

$$\ddot{\vec{r}} = -\frac{q^2}{4m^2\omega^2} \frac{\pi^2 D^2}{L^2} \left(1 - \frac{4D}{3L} \right) \nabla \left(\vec{G}_Q^2 + \vec{G}_D^2 \right), \quad (3.54)$$

which we rewrite as

$$\ddot{\vec{R}} = -\frac{\mu_0^2}{L^2\gamma^2} \nabla \left(\vec{G}_Q^2 + \vec{G}_D^2 \right). \quad (3.55)$$

Therefore the beam's dynamics are described by the effective potential

$$U_{\text{eff}}(r, \varphi) = \frac{\mu_0^2}{L^2\gamma^2} (G_2^2 r^2 + G_6^2 r^{10}). \quad (3.56)$$

The potential (3.56) does not match up with the desired effective potential (3.12), we are missing the cross-term between the components because they are displaced.

3.2 Simulation Results

In the following simulation we consider a realistic beam described by a parabolic distribution in phase space [26], [27],

$$f = f_0 \left(1 - \frac{x^2 + y^2}{2R^2} - \frac{p_x^2 + p_y^2}{2p_0^2} \right), \quad (3.57)$$

which has a projection in configuration space close to a truncated Gaussian distribution:

$$\rho_b = \frac{3I}{2\pi c\beta R^2} \left(1 - \frac{r^2}{2R^2} \right)^2. \quad (3.58)$$

The quadrupole and duodecapole must then satisfy

$$\begin{aligned}\rho_b &= \frac{\epsilon_0}{1 + \delta} \gamma^2 \Delta U_{\text{eff}} \\ &= \frac{2\epsilon_0}{1 + \delta} \frac{\mu_0^2}{L^2} (G_2^2 + 10G_2G_6r^4 \cos(4\varphi) + 25G_6^2r^8) \\ &= G_2^2 \frac{2\epsilon_0}{1 + \delta} \frac{\mu_0^2}{L^2} (1 + 10\zeta r^4 \cos(4\varphi) + 25\zeta^2 r^8),\end{aligned}$$

where $\zeta = \frac{G_6}{G_2}$ and μ_0 is as defined in (3.51). Therefore in order to provide matching [27], we choose

$$G_2 = \frac{\sqrt{8\pi mc^2}}{q\lambda R} \sqrt{\frac{\epsilon^2}{R^2} + \frac{3I}{I_c\beta\gamma}}, \quad (3.59)$$

$$G_6 = -\frac{G_2}{12\beta\gamma R^4} \frac{I}{I_c} \left(\frac{\epsilon^2}{R^2} + \frac{3I}{I_c\beta\gamma} \right)^{-1}. \quad (3.60)$$

The results of the particle-in-cell the simulation of a 150 keV, 100 mA, $0.06\pi\text{cm mrad}$ proton beam with $G_2 = 50\text{kV}/\text{cm}^2$ and $G_6 = -1.9\text{kV}/\text{cm}^2$ are shown in Figure 3.4.

3.3 Conclusions

We have demonstrated that a simple FODO structure with quadrupole and duodecapole components is capable of preventing emittance growth in space charge dominated beams. Such a structure would provide great benefit at facilities such as the proton accelerator at Los Alamos National Laboratory (LANSCE), where beam current is limited by halo formation due to space charge.

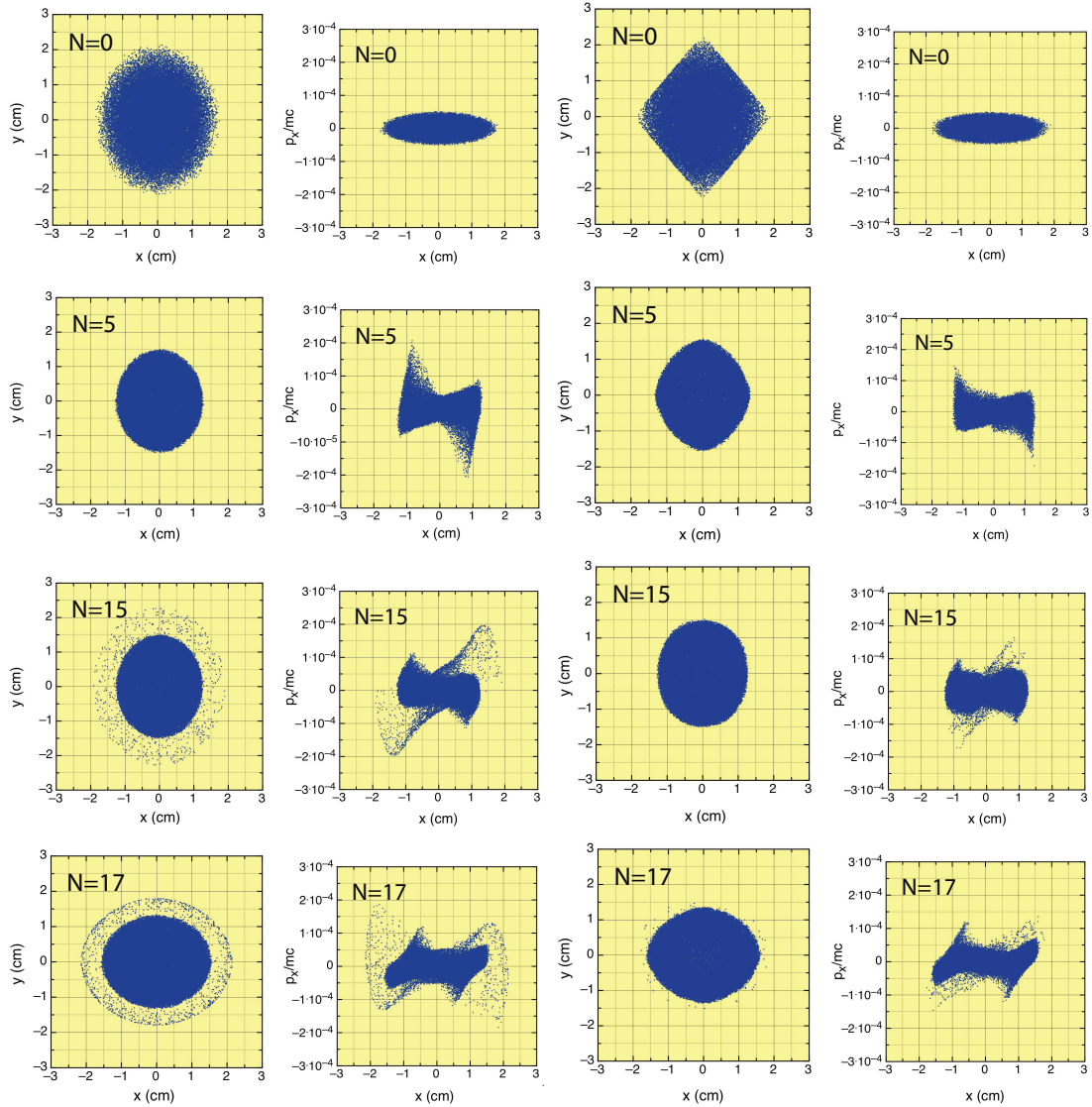


Figure 3.4: Comparison of emittance growth and halo formation (two left columns) and adiabatic matching (two right columns) of the 50 keV, 20 mA, 0.05π cm mrad proton beam in FODO quadrupole channel with the period of $L = 15$ cm, lens length of $D = 5$ cm and field gradient of $G_2 = 1.325$ kV/cm² and adiabatic decline of duodecapole component from $G_6 = -0.005$ kV/cm⁶ to zero for the distance of 7 periods. Numbers indicate FODO periods.

Chapter 4

Rotation Rate Adaptive Tuning

In this chapter, we intuitively motivate our adaptive tuning scheme, rotation rate (RR) tuning [14, 15, 16], which we mathematically justify in the Chapters that follow.

4.0.1 Physical Motivation

It is well known that by adding a fast, small oscillation into a system's dynamics, unexpected stability properties may be achieved. The classic example is of the inverted pendulum, whose vertical equilibrium point may be stabilized by rapidly vertically oscillating the pendulum's pivot point. The dynamics of this process were first analytically described in the 1950s by Kapitza [18]. The adaptive scheme has some similarities to this approach, in that we introduce high frequency oscillations into a system in order to force certain points of the state space to become stable equilibrium points towards which the system's trajectory converges. By abstracting this to a general state space and choosing such a point to be the minimum of a cost function, we are able to tune a wide range of systems towards various performance goals.

We start with a simple example, we do not introduce any destabilizing terms in (4.1), (4.2), which are discussed in remark 3. To give a simple 2D overview of

this method, we consider finding the minimum of a measurable function $C(x, y)$, for which we cannot simply implement a gradient descent for the trajectory of $(x(t), y(t))$ because we are unaware of its analytic form. We propose the following adaptive scheme:

$$\frac{\partial x}{\partial t} = \sqrt{\alpha\omega} \cos(\omega t + kC(x, y)) \quad (4.1)$$

$$\frac{\partial y}{\partial t} = \sqrt{\alpha\omega} \sin(\omega t + kC(x, y)). \quad (4.2)$$

Note that although $C(x, y)$ enters the argument of the adaptive scheme, we do not rely on any knowledge of the analytic form of $C(x, y)$, we simply assume that its value is available for measurement at different locations (x, y) .

The velocity vector,

$$\mathbf{v} = \left(\frac{\partial x}{\partial t}, \frac{\partial y}{\partial t} \right) = \sqrt{\alpha\omega} [\cos(\theta(t)), \sin(\theta(t))], \quad (4.3)$$

$$\theta(t) = \omega t + kC(x(t), y(t)), \quad (4.4)$$

has constant magnitude, $\|\mathbf{v}\| = \sqrt{\alpha\omega}$, and therefore the trajectory $(x(t), y(t))$ moves at a constant speed. However, the rate at which the direction of the trajectories' heading changes is a function of ω , k , and $C(x(t), y(t))$ expressed as:

$$\frac{\partial \theta}{\partial t} = \omega + k \frac{\partial C}{\partial t}. \quad (4.5)$$

Therefore, when the trajectory is heading in the correct direction, towards a decreasing value of $C(x(t), y(t))$, the term $k \frac{\partial C}{\partial t}$ is negative so the overall turning rate $\frac{\partial \theta}{\partial t}$ (4.5), is decreased. On the other hand, when the trajectory is heading in the wrong direction, towards an increasing value of $C(x(t), y(t))$, the term $k \frac{\partial C}{\partial t}$ is positive, and the turning rate is increased. On average, the system ends up approaching the minimizing location of $C(x(t), y(t))$ because it spends more time moving towards it than away.

The ability of this direction-dependent turning rate scheme is apparent in the simulation of system (4.1), (4.2), in Figure 4.1. The system, starting at initial location $x(0) = 1, y(0) = -1$, is simulated for 5 seconds with update parameters $\omega = 50, k = 5, \alpha = 0.5$, and $C(x, y) = x^2 + y^2$. We compare the actual system's (4.1), (4.2) dynamics with those of a system performing gradient descent:

$$\frac{\partial \bar{x}}{\partial t} \approx -\frac{k\alpha}{2} \frac{\partial C(\bar{x}, \bar{y})}{\partial \bar{x}} = -k\alpha \bar{x} \quad (4.6)$$

$$\frac{\partial \bar{y}}{\partial t} \approx -\frac{k\alpha}{2} \frac{\partial C(\bar{x}, \bar{y})}{\partial \bar{y}} = -k\alpha \bar{y}, \quad (4.7)$$

whose behavior our system mimics on average, with the difference

$$\max_{t \in [0, T]} \|(x(t), y(t)) - (\bar{x}(t), \bar{y}(t))\| \quad (4.8)$$

made arbitrarily small for any value of T , by choosing arbitrarily large values of ω . The derivation of this relationship and of the rate of the gradient descent are given in the Chapters that follow.

Towards the end of the simulation, when the system's trajectory is near the origin, $C(x, y) \approx 0$, and the dynamics of (4.1), (4.2) are approximately

$$\frac{\partial x}{\partial t} \approx \sqrt{\alpha\omega} \cos(\omega t) \implies x(t) \approx \sqrt{\frac{\alpha}{\omega}} \sin(\omega t) \quad (4.9)$$

$$\frac{\partial y}{\partial t} \approx \sqrt{\alpha\omega} \sin(\omega t) \implies y(t) \approx -\sqrt{\frac{\alpha}{\omega}} \cos(\omega t), \quad (4.10)$$

a circle of radius $\sqrt{\frac{\alpha}{\omega}}$, which is made arbitrarily small by choosing arbitrarily large values of ω . A detailed overview of how to choose the values k, α , and ω is given in Section 7. Convergence towards a maximum, rather than a minimum is achieved by replacing k with $-k$.

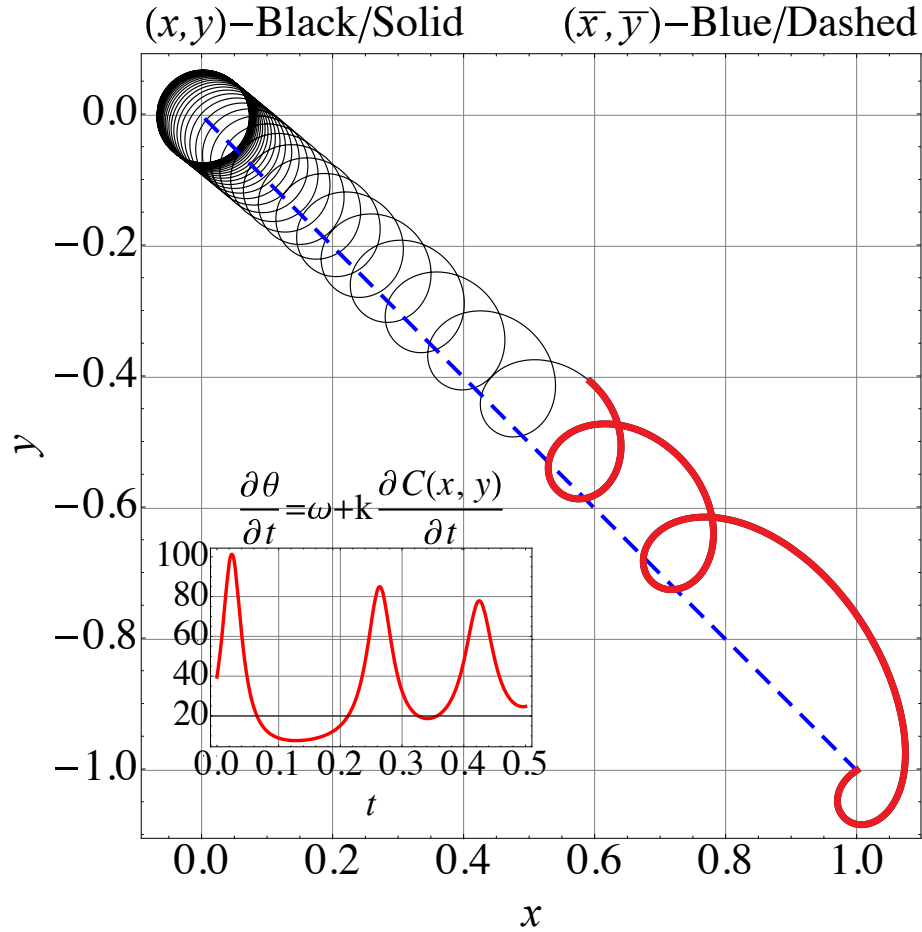


Figure 4.1: The subfigure in the bottom left shows the rotation rate, $\frac{\partial \theta}{\partial t} = \omega + \frac{\partial C(x, y)}{\partial t}$, for the part of the trajectory that is bold red, which takes place during the first 0.5 seconds of simulation. The rotation of the parameters' velocity vector $\mathbf{v}(t)$ slows down when heading towards the minimum of $C(x, y) = x^2 + y^2$, at which time $k \frac{\partial C}{\partial t} < 0$, and speeds up when heading away from the minimum, when $k \frac{\partial C}{\partial t} > 0$. The system ends up spending more time heading towards and approaches the minimum of $C(x, y)$.

Chapter 5

Control Theory Background

The adaptive control method results that we will present perform optimization by maximizing or minimizing a detectable, but analytically unknown cost function. The motivation behind this approach is in stabilizing systems at certain points of their state space, about which analytic results are typically proven using Lyapunov functions. In what follows, we consider cost functions in an analogous manner to Lyapunov functions, and implement controllers which force the stable equilibrium point of the system to be the maximizing or minimizing values for the desired cost functions, in this way we force parameters to converge to optimal values. Before we get into the details of the analysis, we perform a quick review of some technicalities that come up.

5.1 Lyapunov Functions and Stability Theory

5.1.1 Stability

In what follows we deal primarily with systems of the form:

$$\dot{\mathbf{x}} = \mathbf{f}(\mathbf{x}, t) + \mathbf{g}(\mathbf{x}, t)u(\mathbf{x}, t), \quad (5.1)$$

in which $u(\mathbf{x}, t)$ is the control input that we are free to design. For our review of some stability concepts, for notational convenience, we group the two terms on the right side of (5.1) and simply write:

$$\dot{\mathbf{x}} = \mathbf{f}(\mathbf{x}, t), \quad (5.2)$$

keeping in mind that $\mathbf{f}(\mathbf{x}, t)$ may contain the influence of a feedback controller that we have designed.

Remark 1 *For any point $\mathbf{y}_0 \in \mathbb{R}^n$, by translating to a new coordinate system $\mathbf{x} = \mathbf{y} - \mathbf{y}_0$, we translate the equilibrium point to $\mathbf{x} = 0$ without changing the dynamics of system (5.1), therefore, in the definitions that follow, without loss of generality, $\mathbf{x} = 0$ is assumed to be the system's equilibrium point.*

We now present some of the most common forms of stability, with which our analysis is concerned [13]:

Definition 1 *The equilibrium point $\mathbf{x} = 0$ of (5.2) is*

- *stable if, for each $\epsilon > 0$, there is $\delta = \delta(\epsilon, t_0) > 0$ such that*

$$\|\mathbf{x}(t_0)\| < \delta \implies \|\mathbf{x}(t)\| < \epsilon, \quad \forall t \geq t_0 \quad (5.3)$$

- *uniformly stable if, for each $\epsilon > 0$, there is $\delta = \delta(\epsilon) > 0$, independent of t_0 , such that (5.3) is satisfied*
- *asymptotically stable if it is stable and there is a positive constant $c = c(t_0)$ such that $\mathbf{x}(t) \rightarrow 0$ as $t \rightarrow \infty$, for all $\|\mathbf{x}(t_0)\| < c$.*
- *uniformly asymptotically stable if it is uniformly stable and there is a positive constant, c , independent of t_0 , such that for all $\|\mathbf{x}(t_0)\| < c$, $\mathbf{x}(t) \rightarrow 0$ as $t \rightarrow \infty$, uniformly in t_0 .*

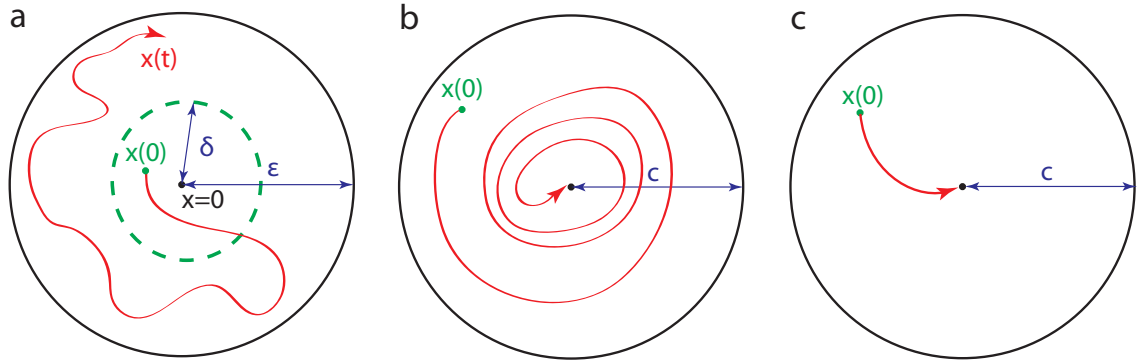


Figure 5.1: Stable (a), asymptotically stable (b), and exponentially stable (c) equilibrium point $\mathbf{x} = 0$.

- *globally uniformly asymptotically stable if it is uniformly and asymptotically stable, globally, regardless of the initial conditions.*
- *exponentially stable if there exist c , k , and $\gamma > 0$ such that*

$$\|\mathbf{x}(t)\| < k \|\mathbf{x}(t_0)\| e^{-\gamma(t-t_0)}, \quad \forall \|\mathbf{x}(t_0)\| < c. \quad (5.4)$$

- *globally exponentially stable if (5.4) holds for all values of $\mathbf{x}(t_0) \in \mathbb{R}^n$.*

5.1.2 Lyapunov Functions

Determining if a system is stable is obvious for a simple system, for which an analytic solution can be found, such as all linear time-invariant systems:

$$\dot{\mathbf{x}} = A\mathbf{x}, \quad (5.5)$$

which can analytically be solved:

$$\mathbf{x}(t) = e^{At}\mathbf{x}(0), \quad (5.6)$$

in which case, the origin is an exponentially stable equilibrium point if and only if all of the eigenvalues of the matrix A have negative real parts, that is, if A is a Hurwitz matrix. For example, the scalar system

$$\dot{x} = -x, \quad (5.7)$$

has the analytic solution

$$x(t) = e^{-t}x(0), \quad (5.8)$$

of which the origin is obviously an exponentially stable equilibrium point. A system of two coupled linear differential equations, such as

$$\dot{x}_1 = -2x_1 + x_2, \quad (5.9)$$

$$\dot{x}_2 = 2x_1 - 3x_2, \quad (5.10)$$

can be re-written in matrix form as:

$$\dot{\mathbf{x}} = \begin{bmatrix} -2 & 1 \\ 2 & -3 \end{bmatrix} \begin{bmatrix} x_1 \\ x_2 \end{bmatrix} = A\mathbf{x}, \quad (5.11)$$

in which the matrix A is Hurwitz, with eigenvalues $\{\lambda_1 = -4, \lambda_2 = -1\}$, and the origin is therefore an exponentially stable equilibrium point.

In the case of a nonlinear system, determining stability is not so straight forward, consider the example of a pendulum, whose equation of motion is given by (setting the length and mass equal to 1 for notational simplicity):

$$\ddot{\theta} = -\sin(\theta) - b\dot{\theta}, \quad (5.12)$$

where the $-b\dot{\theta}$ term is due to damping. From basic physics we know that this system will settle at the equilibrium point $\theta = 0$, after oscillating, as it is continuously slowed by the frictional force. The analytic solution of this system is, however, very

complicated, and one way to prove the stability condition is to consider the total energy of the system, which is given by:

$$E = (1 - \cos(\theta)) + \frac{1}{2}\dot{\theta}^2. \quad (5.13)$$

If we consider the time derivative of the total energy, we get

$$\frac{dE}{dt} = \dot{\theta} \sin(\theta) + \dot{\theta}\ddot{\theta} = \dot{\theta} \sin(\theta) - \dot{\theta} \sin(\theta) - b\dot{\theta}^2 = -b\dot{\theta}^2 < 0, \quad (5.14)$$

and therefore the energy of the system is continuously decreased, as it asymptotically settles to $\dot{\theta} = 0$, at $\theta = 0$.

The idea of a system's energy was generalized by Aleksandr Mikhailovich Lyapunov with his idea of a Lyapunov function:

Definition 2 $V(\mathbf{x}, t)$ is a Lyapunov function for the system:

$$\dot{\mathbf{x}} = \mathbf{f}(\mathbf{x}, t), \quad (5.15)$$

if

$$V(0, t) = 0, \text{ and } V(\mathbf{x} \neq 0, t) > 0.$$

The main stability result that we are interested in, utilizing Lyapunov's generalized energy functions, is then:

Theorem 1 If $\mathbf{x} = 0$ is an equilibrium point of system (5.15) and there exists a Lyapunov function, $V(\mathbf{x}, t)$, and positive constants k_1, k_2, k_3 , and a , such that:

$$k_1 \|\mathbf{x}\|^a \leq V(\mathbf{x}, t) \leq k_2 \|\mathbf{x}\|^a, \quad (5.16)$$

and

$$\begin{aligned}
\frac{dV}{dt} &= \frac{\partial V}{\partial t} + \sum_{i=1}^n \frac{\partial V}{\partial x_i} \frac{\partial x_i}{\partial t} = \frac{\partial V}{\partial t} + \sum_{i=1}^n \frac{\partial V}{\partial x_i} f_i(\mathbf{x}, t) \\
&= \frac{\partial V}{\partial t} + \begin{bmatrix} \frac{\partial V}{\partial x_1} & \frac{\partial V}{\partial x_2} & \cdots & \frac{\partial V}{\partial x_n} \end{bmatrix} \begin{bmatrix} f_1(\mathbf{x}, t) \\ f_2(\mathbf{x}, t) \\ \vdots \\ f_n(\mathbf{x}, t) \end{bmatrix} \\
&= \frac{\partial V}{\partial t} + \frac{\partial V}{\partial \mathbf{x}} \mathbf{f}(\mathbf{x}, t) \leq -k_3 \|\mathbf{x}\|^a,
\end{aligned} \tag{5.17}$$

then $\mathbf{x} = 0$ is exponentially stable.

Example 1 Consider again the system

$$\dot{x}_1 = -2x_1 + x_2, \tag{5.18}$$

$$\dot{x}_2 = 2x_1 - 3x_2, \tag{5.19}$$

and consider the Lyapunov function:

$$V(x_1, x_2) = \frac{1}{2} \|\mathbf{x}\|^2 = \frac{1}{2} x_1^2 + \frac{1}{2} x_2^2, \tag{5.20}$$

which satisfies

$$\begin{aligned}
\dot{V} &= x_1 \dot{x}_1 + x_2 \dot{x}_2 = x_1 (-2x_1 + x_2) + x_2 (2x_1 - 3x_2) = -2x_1^2 + 3x_1x_2 - 3x_2^2 \\
&= -\frac{3}{2} (x_1 - x_2)^2 - x_2^2 - \frac{1}{2} (x_1^2 + x_2^2) < -\frac{1}{2} \|\mathbf{x}\|^2,
\end{aligned} \tag{5.21}$$

and therefore, by Theorem 1, the origin is exponentially stable.

5.2 Weak Convergence

The averaging and stability analysis of the systems which we will consider depend on the functional analysis results of Kurzweil, Jarnik, Sussmann, and Liu [21, 22, 23],

which allows one to relate the trajectories of a highly oscillatory system to those of a simplified Lie bracket averaged system. First, we briefly recall the notion of weak convergence.

For any given time interval of interest $t \in [t_0, t_0 + T]$, we consider the space of integrable functions

$$L^2([t_0, t_0 + T]) = \left\{ u : [t_0, t_0 + T] \rightarrow \mathbb{R} \mid \int_{t_0}^{t_0+T} u^2(t) dt < \infty \right\}, \quad (5.22)$$

and recall the notion of weak convergence:

Definition 3 *A sequence of functions $\{u_n\} \subset L^2([t_0, t_0 + T])$ converges weakly to $u \in L^2([t_0, t_0 + T])$ if*

$$\lim_{n \rightarrow \infty} \int_{t_0}^{t_0+T} u_n(t)v(t) dt = \int_{t_0}^{t_0+T} u(t)v(t) dt, \quad \forall v \in L^2([t_0, t_0 + T]). \quad (5.23)$$

Example 1 *The sequences of functions $\cos(n\omega t)$ and $\cos^2(n\omega t)$ weakly converge to 0 and $\frac{1}{2}$, respectively, that is, according to the Riemann-Lebesgue Lemma, the following limits hold $\forall v \in L^2([t_0, t_0 + T])$:*

$$\lim_{n \rightarrow \infty} \int_{t_0}^{t_0+T} \cos(n\omega t)v(t) dt = \int_{t_0}^{t_0+T} 0v(t) dt = 0, \quad (5.24)$$

$$\lim_{n \rightarrow \infty} \int_{t_0}^{t_0+T} \cos^2(n\omega t)v(t) dt = \int_{t_0}^{t_0+T} \frac{1}{2}v(t) dt = \frac{1}{2} \int_{t_0}^{t_0+T} v(t) dt. \quad (5.25)$$

We now state the general Theorem that we are interested in:

Theorem 2 [21, 22, 23] *For $T \in [0, \infty)$, and a compact set $K \subset \mathbb{R}^n$, consider a sequence $(k \in \mathbb{N})$ of sets of n coupled differential equations $(\mathbf{x} = (x_1, \dots, x_n))$:*

$$\dot{\mathbf{x}} = \mathbf{f}(\mathbf{x}, t) + \sum_{i=1}^n \mathbf{g}_i(\mathbf{x}, t)\varphi_{i,k}(t), \quad \mathbf{x}(0) = \mathbf{x}_0, \quad (5.26)$$

where $\dot{\mathbf{x}}$ denotes $\frac{\partial \mathbf{x}}{\partial t}$ and the functions $\mathbf{f}(\mathbf{x}, t)$, $\mathbf{g}_i(\mathbf{x}, t)$, and $\varphi_{i,k}(t)$ are continuous and Lipschitz, and their first and second derivatives are continuous and bounded. If the

functions $\varphi_{i,k}(t)$ are continuous and their integrals satisfy:

$$\Phi_{i,k}(t) = \int_{t_0}^{t_0+t} \varphi_{i,k}(\tau) d\tau \rightarrow 0 \quad \text{uniformly as } k \rightarrow \infty, \quad (5.27)$$

and there exists measurable functions $\lambda_{i,j}(t)$, which are the weak limits of the functions $\varphi_{j,k}(t)\Phi_{i,k}(t)$, such that

$$\lim_{k \rightarrow \infty} \int_{t_0}^{t_0+t} \varphi_{j,k}(\tau)\Phi_{i,k}(\tau)h(\tau)d\tau = \int_{t_0}^{t_0+t} \lambda_{i,j}(\tau)h(\tau)d\tau, \quad \forall h(t) \in L^2([t_0, t_0+t]). \quad (5.28)$$

Then, for all $t \in [t_0, t_0+T]$ and $\mathbf{x} \in K$, the sequence of solutions of (5.26):

$$\mathbf{x}_k(t) = \mathbf{x}_0 + \int_{t_0}^{t_0+t} \left(\mathbf{f}(\mathbf{x}_k, \tau) + \sum_{i=1}^n \mathbf{g}_i(\mathbf{x}_k, \tau)\varphi_{i,k}(\tau) \right) d\tau \quad (5.29)$$

converges uniformly with respect to k , over $(\mathbf{x}, t) \in K \times [t_0, t_0+T]$ to the solution $\mathbf{x}(t)$ satisfying:

$$\dot{\mathbf{x}} = \mathbf{f}(\mathbf{x}, t) - \sum_{i,j=1}^n \lambda_{i,j}(t) (D\mathbf{g}_i(\mathbf{x}, t)) \mathbf{g}_j(\mathbf{x}, t), \quad \mathbf{x}(0) = \mathbf{x}_0. \quad (5.30)$$

The following special case of Theorem 2 is applied in what follows:

Corollary 1 For $T \in [0, \infty)$, and any compact set $K \subset \mathbb{R}^n$ such that the functions $\mathbf{f}(\mathbf{x}, t)$, $\mathbf{h}_i(\mathbf{x}, t)$, $\mathbf{g}_i(\mathbf{x}, t)$ satisfy the assumptions of Theorem 2, for any $\delta > 0$, there exists ω^* such that for all $\omega_0 > \omega^*$, the trajectory $\mathbf{x}(t)$ of the system

$$\dot{\mathbf{x}} = \mathbf{f}(\mathbf{x}, t) + \sum_{i=1}^n \mathbf{h}_i(\mathbf{x}, t)\sqrt{\omega_i} \cos(\omega_i t) - \sum_{i=1}^n \mathbf{g}_i(\mathbf{x}, t)\sqrt{\omega_i} \sin(\omega_i t), \quad (5.31)$$

and the trajectory $\bar{\mathbf{x}}(t)$ of the system

$$\dot{\bar{\mathbf{x}}} = \mathbf{f}(\bar{\mathbf{x}}, t) - \frac{1}{2} \sum_{i \neq j}^n \left[\frac{\partial \mathbf{g}_j}{\partial \bar{\mathbf{x}}} \mathbf{h}_i - \frac{\partial \mathbf{h}_i}{\partial \bar{\mathbf{x}}} \mathbf{g}_j \right], \quad \bar{\mathbf{x}}(0) = \mathbf{x}(0), \quad (5.32)$$

satisfy the convergent trajectories property:

$$\max_{t \in [t_0, t_0+T]} \|\mathbf{x}(t) - \bar{\mathbf{x}}(t)\| < \delta, \quad (5.33)$$

where $\omega_i = \omega_0 r_i$ such that $r_i \neq r_j, \forall i \neq j$.

Proof 1 *Theorem 2 is satisfied for*

$$\begin{aligned}\varphi_{i,\omega} &= \sqrt{\omega_i} \cos(\omega_i t), & \Phi_{i,\omega}(t) &= \frac{1}{\sqrt{\omega_i}} \sin(\omega_i t) \\ \hat{\varphi}_{i,\omega} &= -\sqrt{\omega_i} \sin(\omega_i t), & \hat{\Phi}_{i,\omega}(t) &= \frac{1}{\sqrt{\omega_i}} \cos(\omega_i t)\end{aligned}$$

such that $\forall h(t) \in L^2([t_0, t_0 + T])$ we get, for mixed terms s.t. $i = j$:

$$\begin{aligned}\lim_{\omega \rightarrow \infty} \int_{t_0}^{t_0+T} \varphi_{i,\omega}(t) \hat{\Phi}_{j,\omega}(t) h(t) dt &= \lim_{\omega \rightarrow \infty} \int_{t_0}^{t_0+T} \cos^2(\omega_i t) h(t) dt = \int_{t_0}^{t_0+T} \frac{1}{2} h(t) dt, \\ - \lim_{\omega \rightarrow \infty} \int_{t_0}^{t_0+T} \hat{\varphi}_{i,\omega}(t) \Phi_{j,\omega}(t) h(t) dt &= \lim_{\omega \rightarrow \infty} \int_{t_0}^{t_0+T} \sin^2(\omega_i t) h(t) dt = \int_{t_0}^{t_0+T} \frac{1}{2} h(t) dt,\end{aligned}$$

for mixed terms s.t. $i \neq j$:

$$\begin{aligned}\lim_{\omega \rightarrow \infty} \int_{t_0}^{t_0+T} \varphi_{i,\omega}(t) \hat{\Phi}_{j,\omega}(t) h(t) dt &= \lim_{\omega \rightarrow \infty} \int_{t_0}^{t_0+T} \cos(\omega_i t) \cos(\omega_j t) h(t) dt = 0, \\ - \lim_{\omega \rightarrow \infty} \int_{t_0}^{t_0+T} \hat{\varphi}_{i,\omega}(t) \Phi_{j,\omega}(t) h(t) dt &= \lim_{\omega \rightarrow \infty} \int_{t_0}^{t_0+T} \sin(\omega_i t) \sin(\omega_j t) h(t) dt = 0,\end{aligned}$$

and for all non-mixed terms:

$$\begin{aligned}\lim_{\omega \rightarrow \infty} \int_{t_0}^{t_0+T} \varphi_{i,\omega}(t) \Phi_{j,\omega}(t) h(t) dt &= \lim_{\omega \rightarrow \infty} \int_{t_0}^{t_0+T} \cos(\omega_i t) \sin(\omega_j t) h(t) dt = 0, \\ - \lim_{\omega \rightarrow \infty} \int_{t_0}^{t_0+T} \hat{\varphi}_{i,\omega}(t) \hat{\Phi}_{j,\omega}(t) h(t) dt &= \lim_{\omega \rightarrow \infty} \int_{t_0}^{t_0+T} \sin(\omega_i t) \cos(\omega_j t) h(t) dt = 0,\end{aligned}$$

and therefore

$$\lambda_{i,j} = \begin{cases} \frac{1}{2} : \text{mixed terms } \varphi_{i,\omega} \hat{\Phi}_{j,\omega}, \hat{\varphi}_{i,\omega} \Phi_{j,\omega} \text{ s.t. } i = j \\ 0 : \text{mixed terms } \varphi_{i,\omega} \hat{\Phi}_{j,\omega}, \hat{\varphi}_{i,\omega} \Phi_{j,\omega} \text{ s.t. } i \neq j \\ 0 : \text{all non - mixed terms } \varphi_{i,\omega} \Phi_{j,\omega}, \hat{\varphi}_{i,\omega} \hat{\Phi}_{j,\omega} \end{cases}$$

To illustrate the application of the above methods, we present two simple examples:

Example 2 *Consider the differential equation:*

$$\dot{x} = \sqrt{\omega} \cos(\omega t) - \sqrt{\omega} \sin(\omega t) x^2, \quad (5.34)$$

by application of Corollary 1, by choosing arbitrarily large values of ω , the trajectory $x(t)$, of (5.34), can be made arbitrarily close to the trajectory $\bar{x}(t)$ of:

$$\dot{\bar{x}} = -\bar{x}, \quad \bar{x}(0) = x(0). \quad (5.35)$$

Example 3 Consider the differential equation:

$$\dot{x} = \sqrt{\omega} \cos(\omega t) - \sqrt{\omega} \sin(\omega t)V(x, t), \quad (5.36)$$

by application of Corollary 1, by choosing arbitrarily large values of ω , the trajectory $x(t)$, of (5.36), can be made arbitrarily close to the trajectory $\bar{x}(t)$ of:

$$\dot{\bar{x}} = -\frac{1}{2} \frac{\partial V}{\partial \bar{x}}, \quad \bar{x}(0) = x(0). \quad (5.37)$$

If $V(x, t)$ happens to be a Lyapunov function for system (5.36), then our average system obeys:

$$\dot{V} = \frac{\partial V}{\partial \bar{x}} \frac{\partial \bar{x}}{\partial t} = \frac{\partial V}{\partial \bar{x}} \left(-\frac{1}{2} \frac{\partial V}{\partial \bar{x}} \right) = -\frac{1}{2} \left\| \frac{\partial V}{\partial \bar{x}} \right\|^2 < 0, \quad (5.38)$$

and therefore the origin of the average system is stable and therefore so is that of the actual system, as the trajectories of the two are arbitrarily close.

Our final example demonstrates the application of the above method for simultaneous tuning of many parameters, for minimization of unknown functions.

Example 4 Consider the differential equations:

$$\dot{p}_1 = \sqrt{\omega_1} \cos(\omega_1 t + C(p_1, p_2, t)), \quad (5.39)$$

$$\dot{p}_2 = \sqrt{\omega_2} \cos(\omega_2 t + C(p_1, p_2, t)), \quad (5.40)$$

where C is an analytically unknown function of two parameters p_1 and p_2 , which we would like to minimize. Using trigonometric identities, we expand the system dynamics as:

$$\dot{p}_1 = \sqrt{\omega_1} \cos(\omega_1 t) \cos(C(p_1, p_2, t)) - \sqrt{\omega_1} \sin(\omega_1 t) \sin(C(p_1, p_2, t)), \quad (5.41)$$

$$\dot{p}_2 = \sqrt{\omega_2} \cos(\omega_2 t) \cos(C(p_1, p_2, t)) - \sqrt{\omega_2} \sin(\omega_2 t) \sin(C(p_1, p_2, t)). \quad (5.42)$$

If $\omega_1 = \omega r_1$ and $\omega_2 = \omega r_2$, such that $r_1 \neq r_2$, by application of Corollary 1, by choosing arbitrarily large values of ω , the trajectory $x(t)$, of (5.36), can be made arbitrarily close to the trajectory $\bar{x}(t)$ of:

$$\dot{\bar{p}}_1 = -\frac{1}{2} \frac{\partial C(\bar{p}_1, \bar{p}_2, t)}{\partial \bar{p}_1} (\sin^2(C(p_1, p_2, t)) + \cos^2(C(p_1, p_2, t))), \quad (5.43)$$

$$\dot{\bar{p}}_2 = -\frac{1}{2} \frac{\partial C(\bar{p}_1, \bar{p}_2, t)}{\partial \bar{p}_2} (\sin^2(C(p_1, p_2, t)) + \cos^2(C(p_1, p_2, t))), \quad (5.44)$$

which simplifies to

$$\dot{\bar{p}}_1 = -\frac{1}{2} \frac{\partial C(\bar{p}_1, \bar{p}_2, t)}{\partial \bar{p}_1}, \quad (5.45)$$

$$\dot{\bar{p}}_2 = -\frac{1}{2} \frac{\partial C(\bar{p}_1, \bar{p}_2, t)}{\partial \bar{p}_2}, \quad (5.46)$$

which we combine as

$$\dot{\bar{\mathbf{p}}} = -\frac{1}{2} \nabla C(\bar{\mathbf{p}}, t), \quad (5.47)$$

and therefore the parameters p_1 and p_2 perform a gradient descent towards a minimizing value of C .

Remark 2 The advantage of putting the unknown cost function $C(\mathbf{p}, t)$ inside the argument of $\cos()$ or $\sin()$ is that the parameter update rate has a known bound $\sqrt{\omega_i}$, despite the unknown analytic form of C .

Chapter 6

General Adaptive Scheme

6.1 Adaptive Feedback for Simultaneous Multi-Parameter Optimization

It is clear to see how the controller developed above can be used for optimization of unknown functions. For general tuning, we consider the problem of locating an extremum point of the function $C(\mathbf{p}, t) : \mathbb{R}^n \times \mathbb{R}^+ \rightarrow \mathbb{R}$, for $\mathbf{p} = (p_1, \dots, p_n) \in \mathbb{R}^n$, which we can measure the value of, but whose analytic form is unknown. For notational convenience, in what follows we sometimes write $C(\mathbf{p})$ or just C instead of $C(\mathbf{p}(t), t)$.

The explanation presented in the previous section used $\sin(\cdot)$ and $\cos(\cdot)$ functions for the x and y dynamics to give circular trajectories. The actual requirement for convergence is for an independence, in the frequency domain, of the functions used to perturb different parameters. In what follows, replacing $\cos(\cdot)$ with $\sin(\cdot)$ throughout makes no difference.

Theorem 3 *Consider the setup shown in Figure 6.1 (for maximum seeking we replace*

6.1 Adaptive Feedback for Simultaneous Multi-Parameter Optimization 10

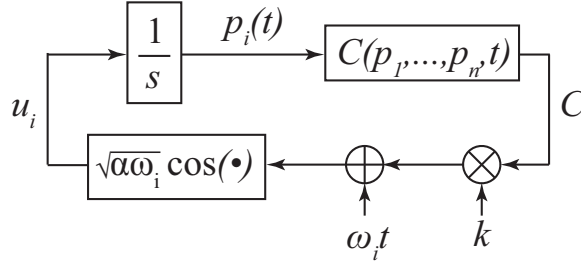


Figure 6.1: Tuning of the i^{th} component p_i of $\mathbf{p} = (p_1, \dots, p_n) \in \mathbb{R}^n$. The symbol $\frac{1}{s}$ denotes the Laplace Transform of an integrator, so that in the above diagram $p_i(t) = p_i(0) + \int_0^t u_i(\tau) d\tau$.

k with $-k$):

$$\dot{p}_i = \sqrt{\alpha\omega_i} \cos(\omega_i t + kC(\mathbf{p}, t)), \quad (6.1)$$

where $\omega_i = \omega_0 r_i$ such that $r_i \neq r_j \ \forall i \neq j$. The trajectory of system (6.1) approaches the minimum of $C(\mathbf{p}, t)$, with its trajectory arbitrarily close to that of

$$\dot{\bar{\mathbf{p}}} = -\frac{k\alpha}{2} \nabla C, \quad \bar{\mathbf{p}}(0) = \mathbf{p}(0) \quad (6.2)$$

with the distance between the two decreasing as a function of increasing ω_0 . Namely, for any given $T \in [0, \infty)$, any compact set of allowable parameters $\mathbf{p} \in K \subset \mathbb{R}^m$, and any desired accuracy δ , there exists ω_0^* such that for all $\omega_0 > \omega_0^*$, the distance between the trajectory $\mathbf{p}(t)$ of (6.1) and $\bar{\mathbf{p}}(t)$ of (6.2) satisfies the bound

$$\max_{\mathbf{p}, \bar{\mathbf{p}} \in K, t \in [0, T]} \|\mathbf{p}(t) - \bar{\mathbf{p}}(t)\| < \delta. \quad (6.3)$$

Proof 2 *By expanding*

$$\cos(\omega_i t + kC) = \cos(\omega_i t) \cos(kC) - \sin(\omega_i t) \sin(kC) \quad (6.4)$$

we rewrite the p_i ($1 \leq i \leq n$) dynamics as

$$\dot{p}_i = \sqrt{\omega_i} \cos(\omega_i t) \sqrt{\alpha} \cos(kC) - \sqrt{\omega_i} \sin(\omega_i t) \sqrt{\alpha} \sin(kC), \quad (6.5)$$

6.1 Adaptive Feedback for Simultaneous Multi-Parameter Optimization 11

and apply Corollary 1 with respect to ω_0 and $\nu = 0.5$. The trajectory of system (6.1) uniformly converges to the trajectory of

$$\begin{aligned}\dot{\bar{p}}_i &= -\frac{k\alpha}{2} \frac{\partial C(\bar{\mathbf{p}}, t)}{\partial \bar{p}_i} (\cos^2(kC(\bar{\mathbf{p}}, t)) + \sin^2(kC(\bar{\mathbf{p}}, t))) \\ &= -\frac{k\alpha}{2} \frac{\partial C(\bar{\mathbf{p}}, t)}{\partial \bar{p}_i},\end{aligned}\tag{6.6}$$

where we have used the fact that mismatched terms of the form $\cos(\omega_i t) \sin(\omega_j t)$, $\forall i, j$, and terms of the form $\cos(\omega_i t) \cos(\omega_j t)$, and $\sin(\omega_i t) \sin(\omega_j t)$, $\forall i \neq j$ weakly, uniformly converge to zero. Combining all the p_i components we get:

$$\dot{\bar{\mathbf{p}}} = -\frac{k\alpha}{2} \nabla C.\tag{6.7}$$

Remark 3 The stability of this scheme is verified by the fact that an addition of an un-modeled, possibly destabilizing perturbation of the form $\mathbf{f}(\mathbf{p}, t)$ to the dynamics of $\dot{\mathbf{p}}$ results in the averaged system:

$$\dot{\bar{\mathbf{p}}} = \mathbf{f}(\bar{\mathbf{p}}, t) - \frac{k\alpha}{2} \nabla C,\tag{6.8}$$

which may be made to approach the minimum of C , by choosing $k\alpha$ large enough relative to the values of $\|(\nabla C)^T\|$ and $\|\mathbf{f}(\bar{\mathbf{p}}, t)\|$. Detailed stability analysis is available in [12].

Remark 4 Although it is glossed over in the averaging analysis presented above, if one looks into the details of the proof of Theorem 2, in the case of a time-varying max/min location $\mathbf{p}^*(t)$ of $C(\mathbf{p}, t)$, there will be terms of the form:

$$\frac{1}{\sqrt{\omega}} \left| \frac{\partial C(\mathbf{p}, t)}{\partial t} \right|,\tag{6.9}$$

which are made to approach zero by increasing ω . Furthermore, in the analysis of the convergence of the error $\mathbf{p}_e(t) = \mathbf{p}(t) - \mathbf{p}^*(t)$ there will be terms of the form:

$$\frac{1}{k\alpha} \left| \frac{\partial C(\mathbf{p}, t)}{\partial t} \right|.\tag{6.10}$$

6.1 Adaptive Feedback for Simultaneous Multi-Parameter Optimization 42

Together, (6.9) and (6.10) imply the intuitively obvious fact that for systems whose time-variation is fast, in which the minimum towards which we are descending is quickly varying, both the value of ω and of the product $k\alpha$ must be larger than for the time-invariant case.

Remark 5 *In the case of different parameters having vastly different response characteristics and sensitivities (such as when tuning both RF and magnet settings in the same scheme), the choices of k and α may be specified differently for each component p_i , as k_i and α_i , without change to the above analysis.*

6.1.1 Multi-Objective Optimization

One of the strengths of the above described method is that multi-objective optimization is easily implemented by simply defying a cost function which takes each objective into account, with different weights for each objective chosen depending on the desired results. Comparing the results of several optimizations, with varying weighs between different objectives then gives the user the same type of choice amongst results, as is typically done with genetic algorithms.

Given m objectives O_1, O_2, \dots, O_m , which correspond to the minimization of m costs C_1, C_2, \dots, C_m , the adaptive scheme is applied as:

$$\dot{p}_i = \sqrt{\alpha\omega_i} \cos(\omega_i t + C_{\text{mo}}(\mathbf{p}, t)), \quad \text{where} \quad C_{\text{mo}}(\mathbf{p}, t) = \sum_{j=1}^m k_m C_m(\mathbf{p}, t), \quad (6.11)$$

where the k_m values are weights chosen by the user, in order to emphasize the importance of one objective over another. The trajectory of system (6.11) approaches the minimum of $C_{\text{mo}}(\mathbf{p}, t)$, with its trajectory arbitrarily close to that of

$$\dot{\bar{\mathbf{p}}} = -\frac{\alpha}{2} \nabla C_{\text{mo}}, \quad \bar{\mathbf{p}}(0) = \mathbf{p}(0) \quad (6.12)$$

6.2 Some Discussion on the RR Method

RR is related to dithering-based optimization/stabilization schemes, known in control theory as extremum seeking (ES), which have been used for optimizing unknown outputs of known, stable, systems, by tuning known controllers. Originally introduced in 1922 [10], an overview of its development is available in [11]. Recently, ES has been extended to perform stabilization and optimization of unknown, possibly unstable systems [12]. RR is a further improvement and modification of those results [14].

There are many existing model dependent numerical methods for multi-dimensional / multi-parameter optimization, such as GA, MOGA, Newton-Raphson and gradient descent based on the analytic form of ∇C . Many optimization methods are actually built into existing accelerator design codes [17]. Since accelerators have many coupled parameters, they are prime candidates for genetic algorithm (GA) and multi-objective genetic algorithm (MOGA) based multidimensional, nonlinear optimization schemes. In fact, MOGAs and GAs have been used to successfully optimize many aspects of particle accelerators, such as magnet and radio frequency (RF) cavity design [1], photoinjector design [2], damping ring design [3], storage ring dynamics [4], global optimization of a lattice [5], neutrino factory design [6], simultaneous optimization of beam emittance and dynamic aperture [7], and free electron laser linac drivers [8]. A thorough review of GA for accelerator physics applications is given in [9].

The main strengths of RR is its model independent nature and ability to deal with multiple parameters simultaneously, even for time-varying systems, such as thermal cycling, or unexpected component damage. Some very simple, but computationally intensive and inefficient, model-independent methods are grid and random point searches, especially for systems with many parameters. Gradient descent, based on a numerical approximation of an unknown ∇C is another model-independent approach, but especially in the case of a multi-parameter, noisy calculation of C , may

face difficulties, whereas RR is both robust to noise in C and does not need to try and estimate ∇C . Only samples $C(n)$ are required.

Simplex Fitting, in the sense that it samples many different directions in multi-dimensional parameter space, has the most in common with RR. A major benefit of RR is that its complexity does not grow with parameter number, regardless of the number of parameters being tuned. The scheme basically depends on three choices, the values of k , ω , and α . Regarding noisy data, the RR scheme is, on average, not influenced by noise, unless it happens to both match an RR parameter's perturbation frequency and be large in magnitude relative to that perturbation. Also, noise is easily handled by standard methods, such as averaging and filtering.

Although RR is model independent and able to tune many parameters simultaneously, unlike GA, it is a local technique, similar to gradient descent, and may become trapped in local minimums. Therefore, we plan on exploring (in future work) a combination of GA and RR, in which a GA is first used for global optimization followed by RR for local, in-hardware tuning, to make up for modeling errors and time variation.

Chapter 7

Guidelines for Digital Implementation

7.0.1 Cost and Constraints

The first step is to choose tunable machine parameters, $\mathbf{p} = (p_1, \dots, p_m)$ and a cost function to be minimized, $C = C(p_1(t), \dots, p_m(t), t)$. Next, constraints for all parameters are chosen

$$\mathbf{p}_{\max} = (p_{1,\max}, \dots, p_{m,\max}),$$

$$\mathbf{p}_{\min} = (p_{1,\min}, \dots, p_{m,\min}).$$

Implementing initial parameter settings $\mathbf{p}(1)$, which are chosen based on the physics model and numerical methods, allows one to calculate $C(\mathbf{p}(1))$. The iterative update scheme is then:

$$p_i(n+1) = p_i(n) + \Delta \sqrt{\alpha \omega_i} \cos(\omega_i n \Delta + kC(\mathbf{p}(n))), \quad (7.1)$$

which is based on the finite difference approximation of the derivative:

$$\frac{p_i(t+\Delta) - p_i(t)}{\Delta} \approx \frac{\partial p_i}{\partial t} = \sqrt{\alpha \omega_i} \cos(\omega_i t + kC(\mathbf{p}(t), t)), \quad (7.2)$$

which, according to Theorem 3 will drive the system towards a minimum of C . The constraints are implemented by checking the updated parameters at each step and confining them to their bounds if necessary:

$$\begin{array}{ll} \mathbf{IF} & p_i(n+1) > p_{i,\max}, & \mathbf{THEN} & p_i(n+1) = p_{i,\max}, \\ \mathbf{IF} & p_i(n+1) < p_{i,\min}, & \mathbf{THEN} & p_i(n+1) = p_{i,\min}. \end{array}$$

7.0.2 Choice of ω , and Δ

It is important that $\omega_i \gg kC$, so that the adaptive scheme is operating on a faster time scale than and able to adapt to time variation of the cost function. Because RR depends on distinguishing between different frequency components of the cost, Δ should be chosen in the range of:

$$\Delta \approx \frac{2\pi}{40 \times \max\{\omega_i\}}, \quad (7.3)$$

ensuring that at least 40 iterations ($20 \times$ the Nyquist sampling rate) are required to perform one complete cosine oscillation in the iterative scheme (7.1). Choosing smaller values of Δ results in smoother parameter oscillation and more iterative steps required for convergence, larger values of Δ speed up the convergence, but may destabilize the overall scheme.

According to Theorem 3, the only requirement on the choices of ω_i is that they are big enough and distinct, but in practice, the more harmonically independent they are (such as $\omega_i \neq 2\omega_j$ for all $i \neq j$) the better. The sensitivity to frequency independence is different for every system and depends on the coupling between different components. One simple method is to choose a scaling factor, ω_0 , and

$$\omega_i = \omega_0 r_i, \quad (7.4)$$

where the values r_i are distinct.

The update scheme (7.1) is only valid as a finite difference approximation as in (7.2) if $\Delta \ll 1$ and $\omega_i \gg \sqrt{\alpha}, kC$. Taking into account (7.3), we choose a large value of ω_0 , relative to kC , typically at least

$$\frac{\min \{\omega_i\}}{kC(\mathbf{p}(1))} > 20, \quad (7.5)$$

is a safe choice, where $C(\mathbf{p}(1))$ is the initial cost calculated based on initial parameter settings $\mathbf{p}(1)$.

These choices may vary from system to system based on sensitivity. A good approach is to fix values of k and α , define the various relationships (7.3) - (7.5), and increase ω_0 if necessary.

7.0.3 Choice of k and α

The rate of convergence is proportional to the product $k\alpha$, increasing either k or α speeds up convergence, as long as they are not too big relative to the value of ω_0 , so that the finite difference is an accurate approximation of the derivative. If, after ω_0 has been chosen, the convergence is too slow, or if a local minimum is suspected, k or α may be increased, with the possible need to increase ω_0 as well. The vector \mathbf{p} is moving through the parameter space \mathbb{R}^m in ellipses with approximate major axes of magnitude $\sqrt{\frac{\alpha}{\omega}}$, increasing α causes larger steady state parameter oscillations, which is not a problem if the adaptation is turned off following successful convergence.

7.0.4 Digital Resolution

Although the analytic form of $C(n)$ may be unknown, at each iteration the parameters are perturbed by a quantities with known bounds:

$$0 \leq |\Delta \sqrt{\alpha \omega_i} \cos(\omega_i n \Delta + kC(\mathbf{p}(n)))| \leq \Delta \sqrt{\alpha \omega_{\max}}. \quad (7.6)$$

For a system with n_b bits of resolution, and maximum bounds $\pm M_i$ on the parameter settings, if Δ , α , and ω_i are chosen such that $\Delta\sqrt{\alpha\omega_i} \geq N \times \frac{M_i}{2^{n_b}}$, then, as $\cos(\cdot)$ varies between 0 and 1, it is possible for the parameter value to take N discrete steps of minimum resolution $\frac{M_i}{2^{n_b}}$.

7.0.5 Normalization of Parameters

Different parameters p_i may require individual values of k_i and α_i , in which case normalizing the parameters to within $[-1, 1]$ bounds may be useful. For example, at each step n , one may compute the cost $C(n)$ based on parameter settings $\mathbf{p}(n)$, then translate into the scaled parameters $\mathbf{p}_s(n)$:

$$p_{s,i}(n) = \frac{2(p_i(n) - C_{p,i})}{D_{p,i}}, \quad (7.7)$$

where $C_{p,i} = \frac{p_{i,\max} + p_{i,\min}}{2}$ and $D_{p,i} = p_{i,\max} - p_{i,\min}$, bounding each parameter within $[-1, 1]$. We then perform the RR-update

$$p_{s,i}(n+1) = p_{s,i}(n) + \Delta\sqrt{\alpha_i\omega_i} \cos(\omega_i n \Delta + k_i C(\mathbf{p}(n))), \quad (7.8)$$

force the scaled parameters to satisfy the constraints -1 and 1 , and transform back into un-scaled parameter values in order to calculate the cost for the next iteration:

$$p_i(n+1) = \frac{p_{s,i}(n+1)D_{p,i}}{2} + C_{p,i}. \quad (7.9)$$

Chapter 8

Simulation Results

8.1 Tuning 22 Quadrupole Magnets and 2 Buncher Cavities

In this section we present simulation results of using the RR scheme to tune up the twenty two quadrupole magnets and two buncher cavities in the Los Alamos linear accelerator H^+ transport region, a simplified schematic of which is shown in Figure 8.1. The simulations were done using a GPU-accelerated online beam dynamics simulator [19, 20], which is being developed to predict beam properties along the linac using real time machine parameters. It can serve as a virtual beam experiment environment and contribute to the cost being minimized by the RR optimizer, by providing pseudo realtime estimates of beam sizes and current information in parts of the machine where diagnostics are not available. Currently being demonstrated on the LANSCE low energy beam transport (LEBT) and drift tube linac (DTL), simulating a bunch of 32K macro particles through the LEBT or DTL takes fractions of a second, which is 40 times faster than the simple CPU version of the code.

8.1.1 Magnet Tuning for Beam Transport

In a first, simple demonstration of the technique, we perform a simulation of only the LEBT, with all initial magnet current set points set to $0A$, and allowed to tune up based purely on the RR scheme as described above, in which the four costs ($j=1,2,3,4$) being minimized:

$$C_j = (I_j - 0.013)^2, \quad (8.1)$$

were the square of the difference between initial beam current $0.013A$ and total current making it through various parts of the transport region, at which diagnostics are available. With reference to Figure 8.1, the current is sampled at four locations, I_1 , following Q_6 , I_2 following Q_{10} , I_3 following Q_{18} and I_4 at the end of the transport region. The magnets ($i=1,\dots,22$) were then updated according to:

$$Q_i(n+1) = Q_i(n) + \sqrt{\alpha\omega_i}\Delta \cos(\omega_i\Delta n + kS_i(n)), \quad (8.2)$$

where $S_i = C_4 + C_3 + C_2 + C_1$ for $Q_1 - Q_6$, $S_i = C_4 + C_3 + C_2$ for $Q_7 - Q_{10}$, $S_i = C_4 + C_3$ for $Q_{11} - Q_{18}$ and $S_i = C_4$ for $Q_{19} - Q_{22}$, so that magnets only saw costs which they were able to influence. For the tuning parameters, we chose $k = 250000$, so that the amplified costs kS_j in (8.2) took values between 0 and 300. The ω_i were chosen as $\omega_0 r_i$, with $\omega_0 = 1000$ and r_i uniformly distributed between 2.5 and 3.7, $\Delta = \frac{2\pi}{20\omega_{22}}$, and $\alpha = 15$. With these values, $\frac{\omega_{\min}}{kC_{\max}} > 20$.

Figure 8.2 shows the evolution of the surviving beam current at the end of the transport region during the RR tuning scheme. Figure 8.3 shows the evolution of the magnet current inputs. Figure 8.4 shows the RMS beam size through various parts of the transport region at the end of RR tuning, and Figure 8.5 compares the RR found magnet settings to that of the tune up in 2011.

This example demonstrates some of the strengths and limitations of the scheme, and the importance of cost function choice. Although the cost has been minimized

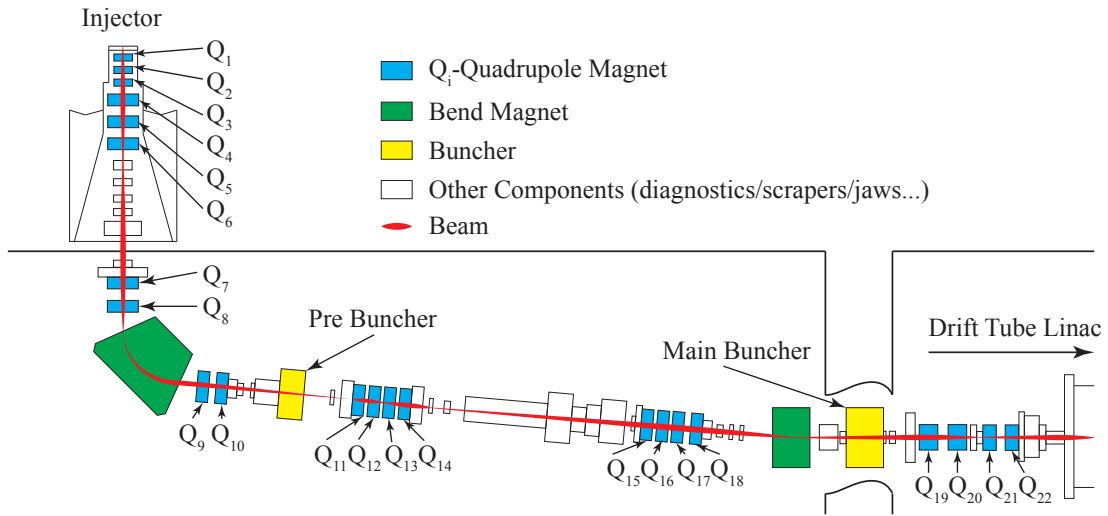


Figure 8.1: Simplified schematic of the LANSCE H^+ injector and transport region.

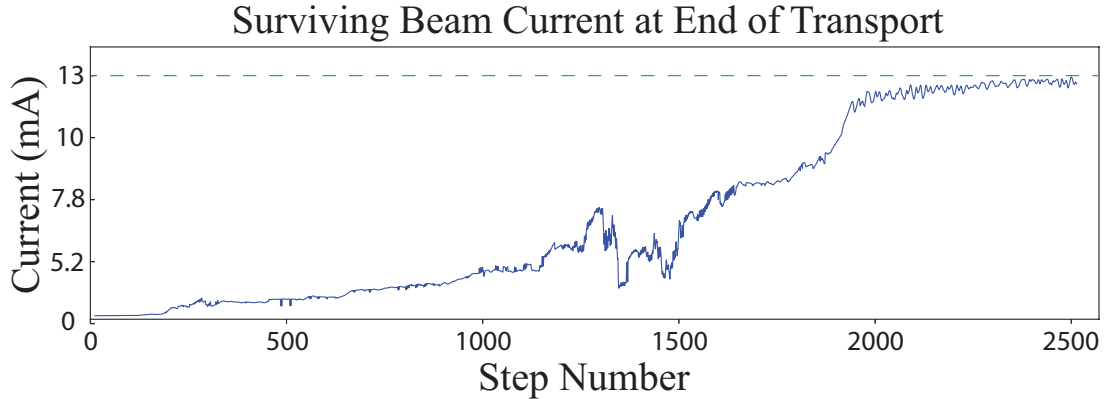


Figure 8.2: The surviving current at the end of the beam transport over 2500 iteration steps is shown for an initial beam current of 13mA.

and almost all current is making it to the end of the transport region, the beam is beginning to diverge and in this form would not be matched to the DTL following the

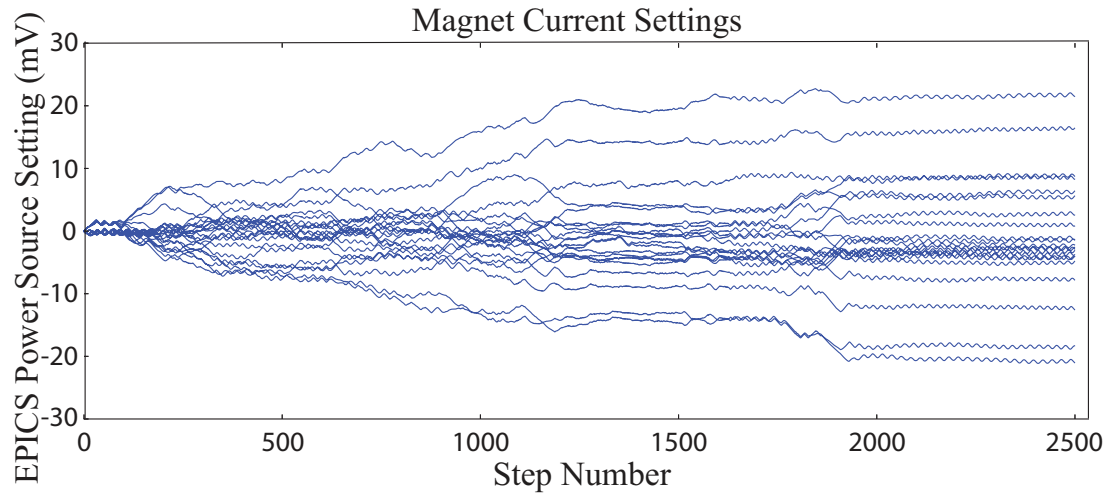


Figure 8.3: Evolution of the magnet current settings to the magnets over 2500 iteration steps.

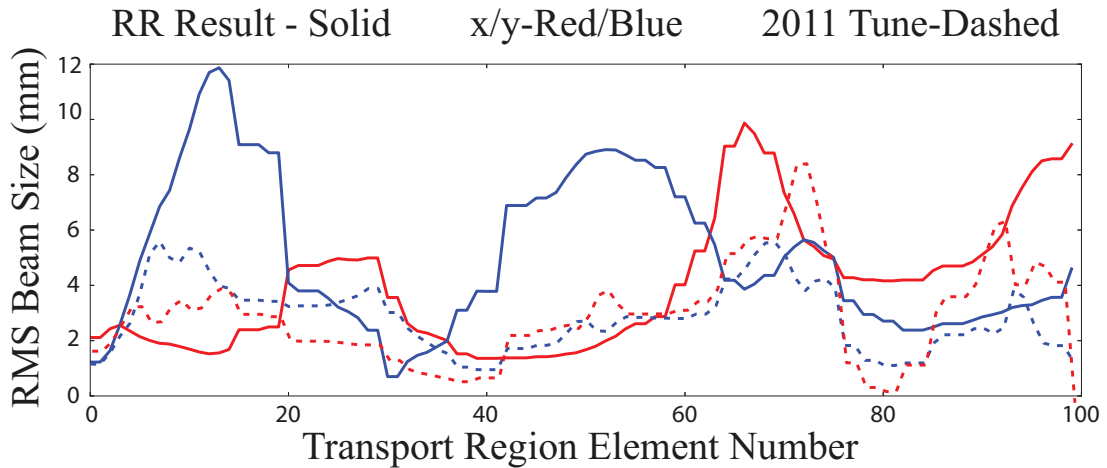


Figure 8.4: RMS beam size at the end of the iterative tuning scheme.

transport region. In practice it is of course better to start with physics-model based initial parameters, this simulation was conducted starting with all magnet settings

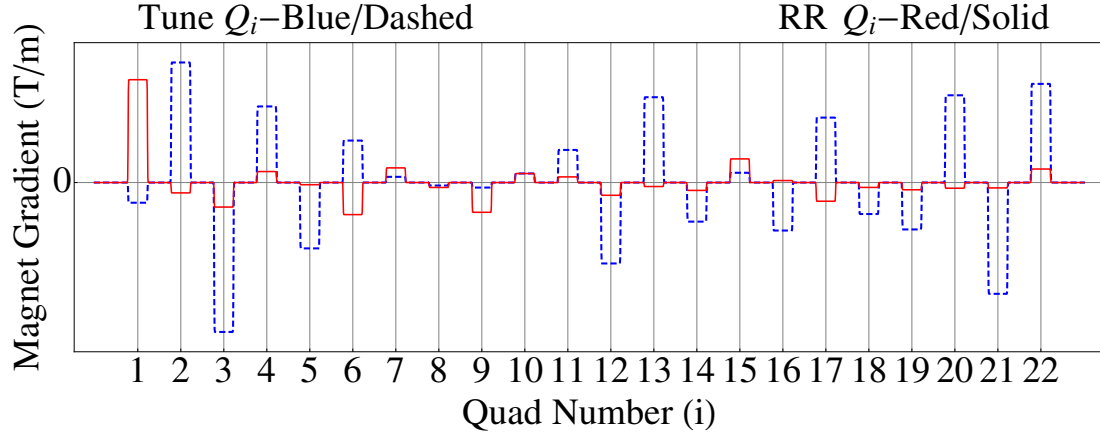


Figure 8.5: Magnet settings at the end of the iterative tuning scheme compared to 2011 tune up settings.

at zero in order to fairly demonstrate the model-independent abilities of the RR scheme. The next simulations start with the 2011 tune up for the magnet settings and use current monitors following two tanks of the DTL, in which case surviving beam corresponds with well-matched beam.

8.1.2 Magnet and RF Buncher Cavity Tuning

To demonstrate the use of this scheme for fine tuning of machine settings, we used machine settings found during the 2011 tune up procedure, but with a slightly different beam and incorrectly phased buncher cavities. The magnets were initialized to the values recorded from one of the 2011 machine turn on tuning periods. We set the phase settings for the buncher and pre-buncher to zero, which typically must be re-tuned at each turn on, by a phase scan, to take care of arbitrary phase shift.

We used only the surviving current at the end of the second tank of the drift tube

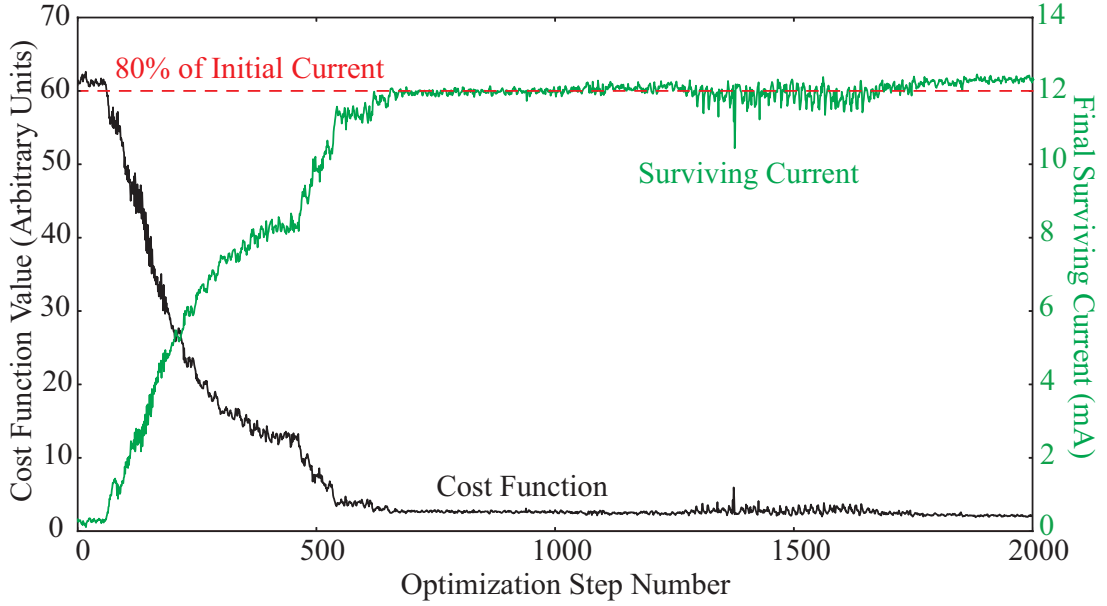


Figure 8.6: The surviving current at the end of the beam transport over 2000 iteration steps is shown for an initial beam current of 15mA.

linac to create our cost, our tuning procedure for the parameters was:

$$Q_i(n+1) = Q_i(n) + \sqrt{\alpha_i \omega_i} \Delta \cos(\omega_i n \Delta + kC(n)), \quad (8.3)$$

where $\alpha_i = \alpha_m$ for the magnets and $\alpha_i = \alpha_b$ for the buncher phases. In both cases

$$C(n) = (I_{\text{end}} - 15\text{mA})^2.$$

For the tuning parameters, we chose $k = 605000$, $\alpha_m = 25$, $\alpha_b = 550$. The ω_i were chosen as $\omega_0 r_i$, with $\omega_0 = 2000$ and r_i uniformly distributed between 2.5 and 4.3, $\Delta = \frac{2\pi}{20\omega_{24}}$. With these values, $\frac{\omega_{\min}}{kC_{\max}} > 35$.

With an initial beam current of 15mA, the typical surviving current after machine tune up is roughly 80% or 12mA. After 2000 simultaneous iterations on these 24

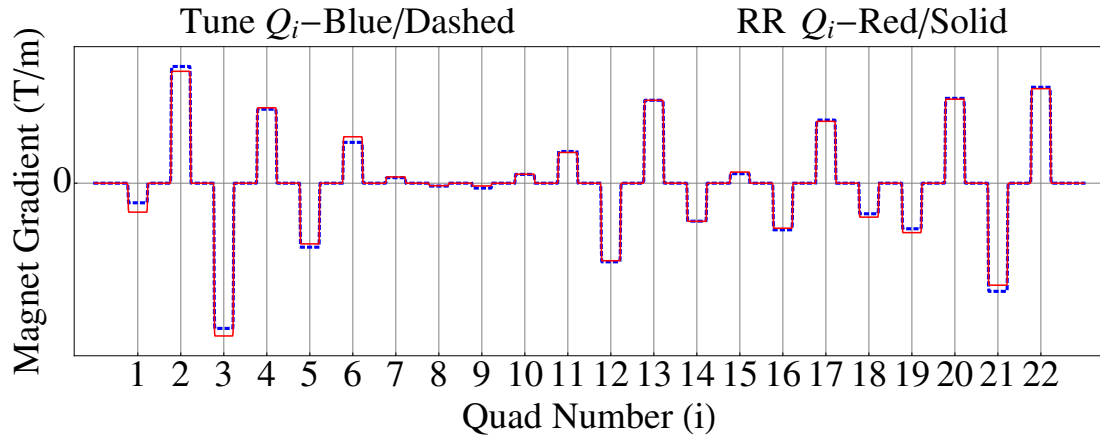


Figure 8.7: New magnet settings after optimization.

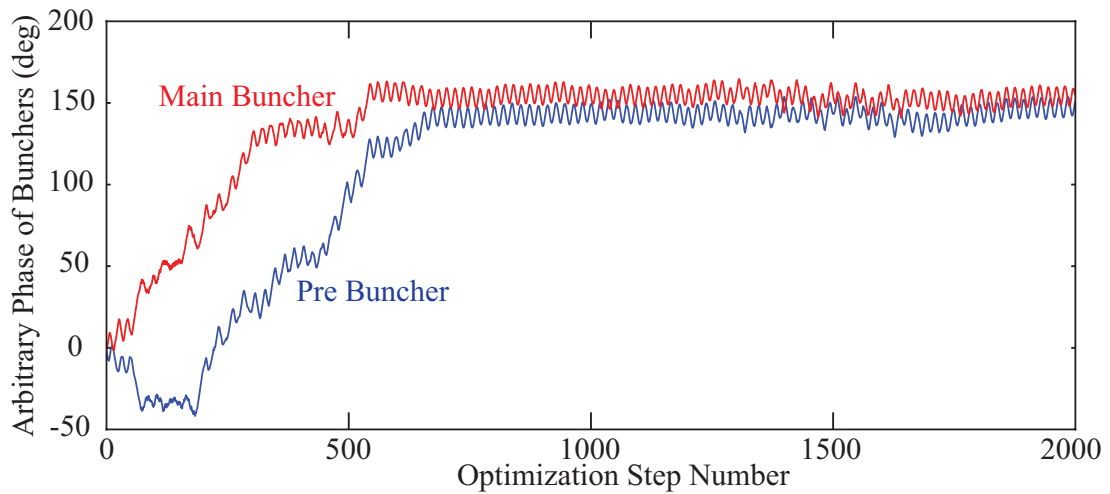


Figure 8.8: Evolution of buncher cavity phase settings over 2000 iteration steps.

parameters (22 quads, 2 buncher phases), the surviving current at the end of Tank 2 was 12.25mA. The results of the optimization procedure are shown in Figures 8.6 -

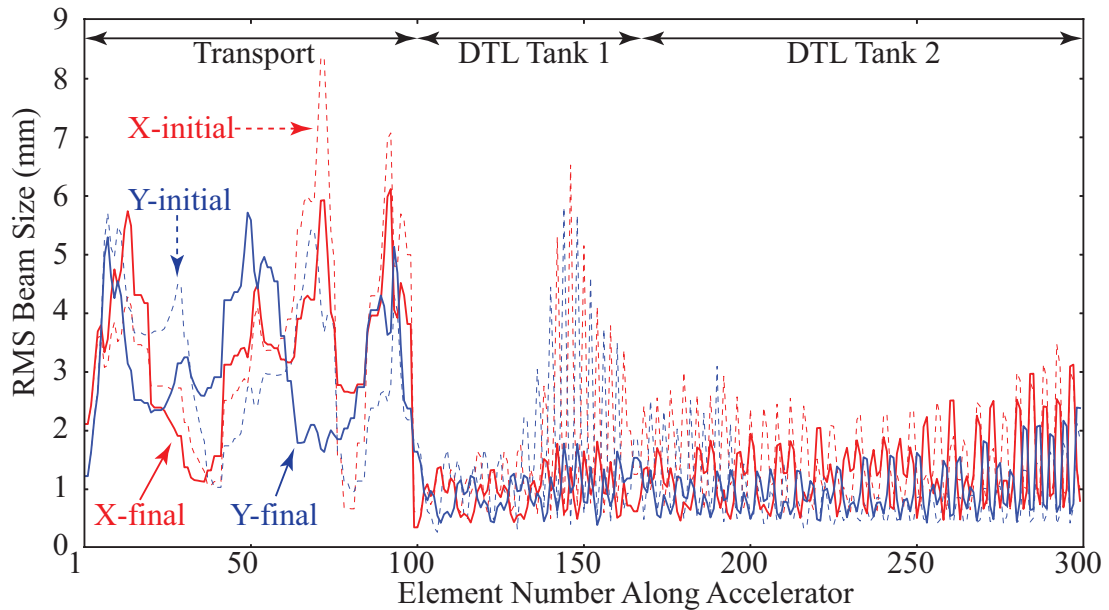


Figure 8.9: Comparison of RMS beam size along the accelerator for the 2011 tune-based magnet settings and arbitrary phase (dashed) with RMS beam size following RR tune (solid).

8.10. From Figures 8.7, 8.8 we see that only minor adjustments are made to magnet settings compared to the RF phases. Figure 8.9 shows that the transverse beam size has further focused throughout the transport region and the transverse match to the DTL has slightly improved. Figure 8.10 compares surviving beam current at the end of Tank 2 of the DTL before and after tuning.

8.1.3 Adaptation to Time Varying Phase Delay and Beam Characteristics

In order to demonstrate the adaptive tuning abilities of the scheme, we started with matched beam settings and varied both the characteristics of the input beam and

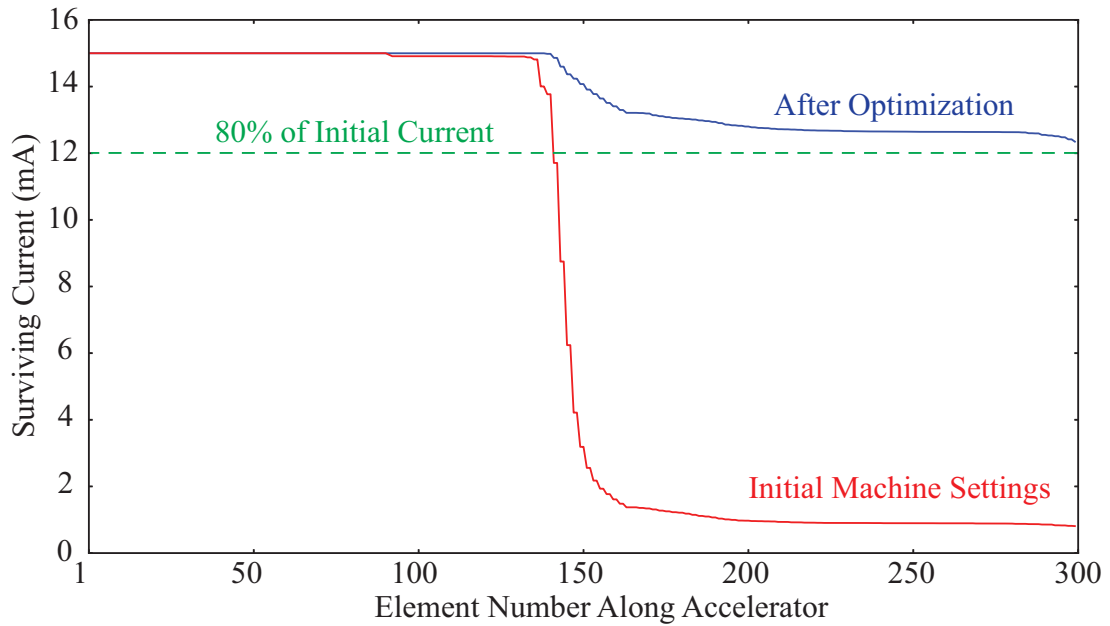


Figure 8.10: Surviving beam current along the machine with 2011 tune-based magnet settings and arbitrary phase (red) and following RR tune (blue).

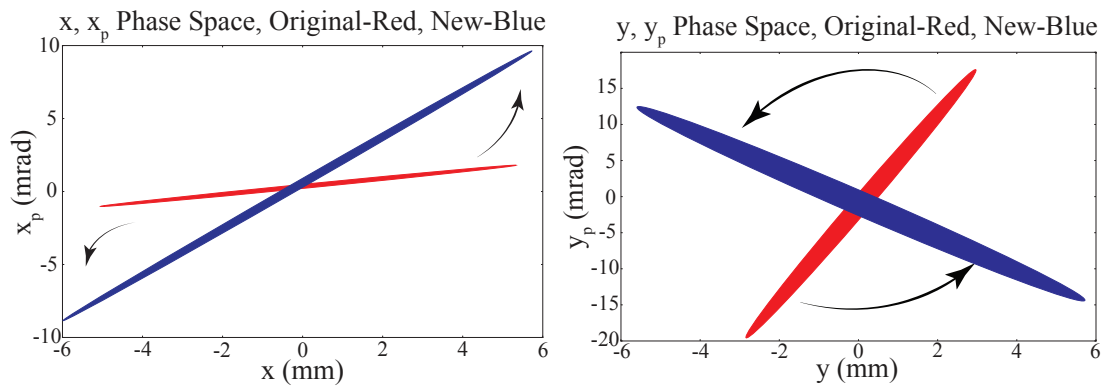


Figure 8.11: The input beam was gradually changed over 18000 time steps.

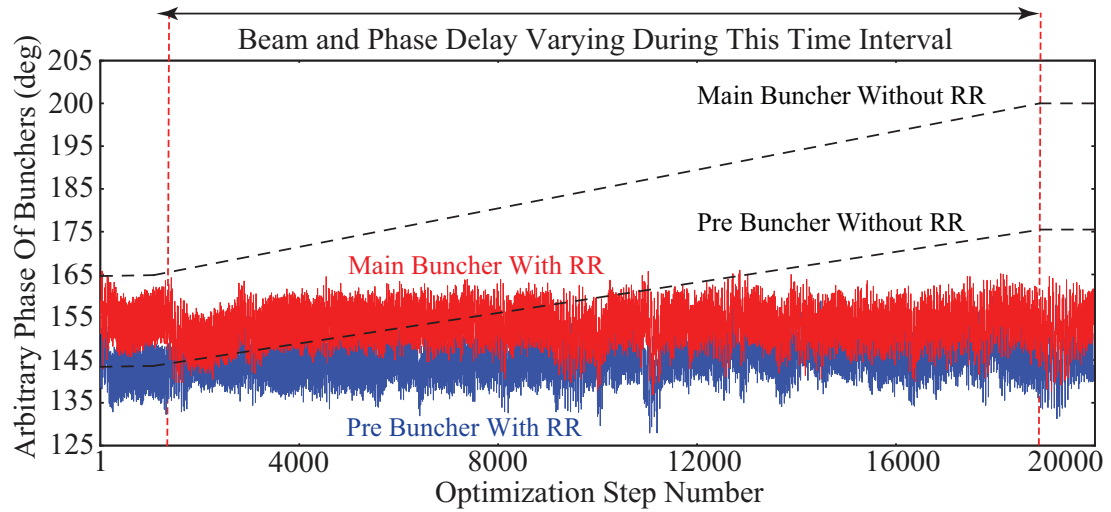


Figure 8.12: Evolution of the buncher phase settings, during, and after variation of beam and phase delay parameters.

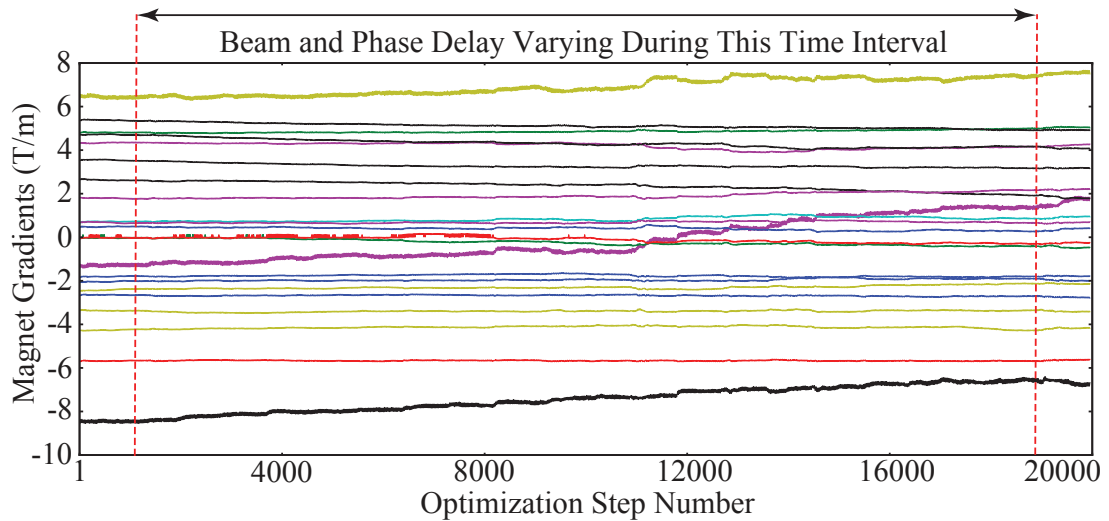


Figure 8.13: Evolution of the magnet gradients before, during, and after variation of beam and phase delay parameters.

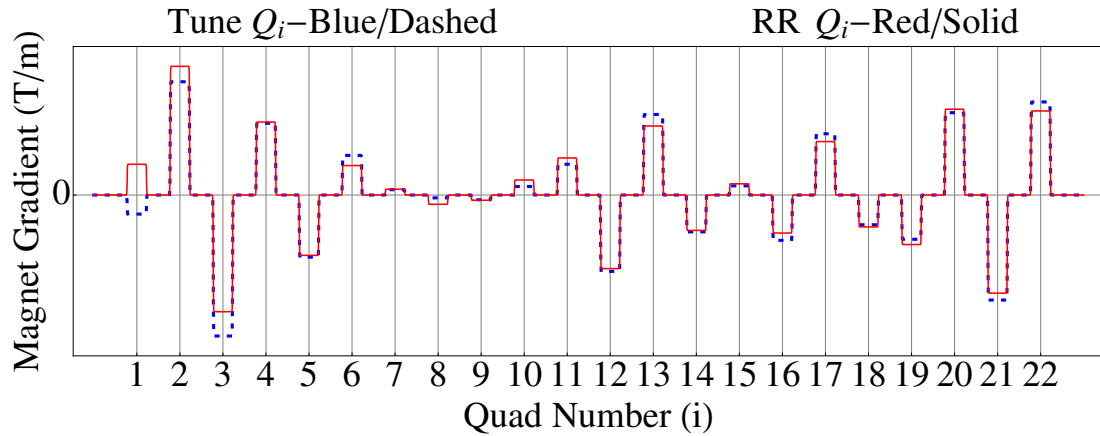


Figure 8.14: New magnet settings after optimization.

added a time-varying phase drift to each buncher cavity.

Figures 8.11 shows the initial and final beam properties at the entrance to the transport region, during which RR adaptive tuning maintains beam focus and matching. Figure 8.12 shows the phase shift of the bunchers with and without tuning. These changes took place starting at step 1000 and finished at step 19000, with beam properties staying constant before and after the interval. Also, during this beam changing process, the phase of the first buncher was made to drift by 30 deg and that of the second by 35 deg, as seen in Figure 8.12. The drift of beam characteristics and buncher phase shifts took place over 18000 time steps, which for a conservative magnet/phase update rate of $1Hz$ translates into drastically changing accelerator and beam properties over the course of just 5 hours. All tuning parameters were maintained exactly the same as in the previous example.

Figure 8.13 shows the evolution of the magnet gradients throughout the process, Figure 8.14 shows the new final magnet settings, and Figure 8.15 compares the initial

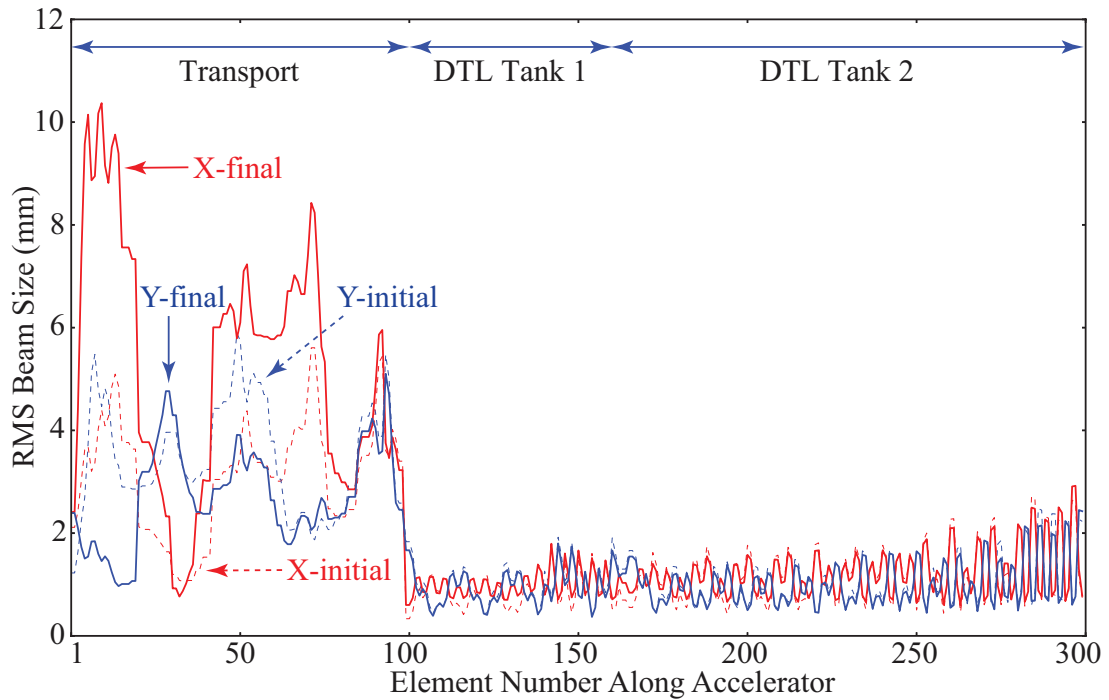


Figure 8.15: Comparison of RMS beam size along the accelerator for the 2011 tune-based magnet settings (dashed) and after the beam initial conditions have changed and RR tuning has re-focused and matched the beam (solid).

and final beam profiles. In Figure 8.16 we see that adaptive RR tuning is able to maintain $\sim 12\text{mA}$ of surviving beam during the time-varying beam and phase, whereas almost all of the beam is lost without tuning.

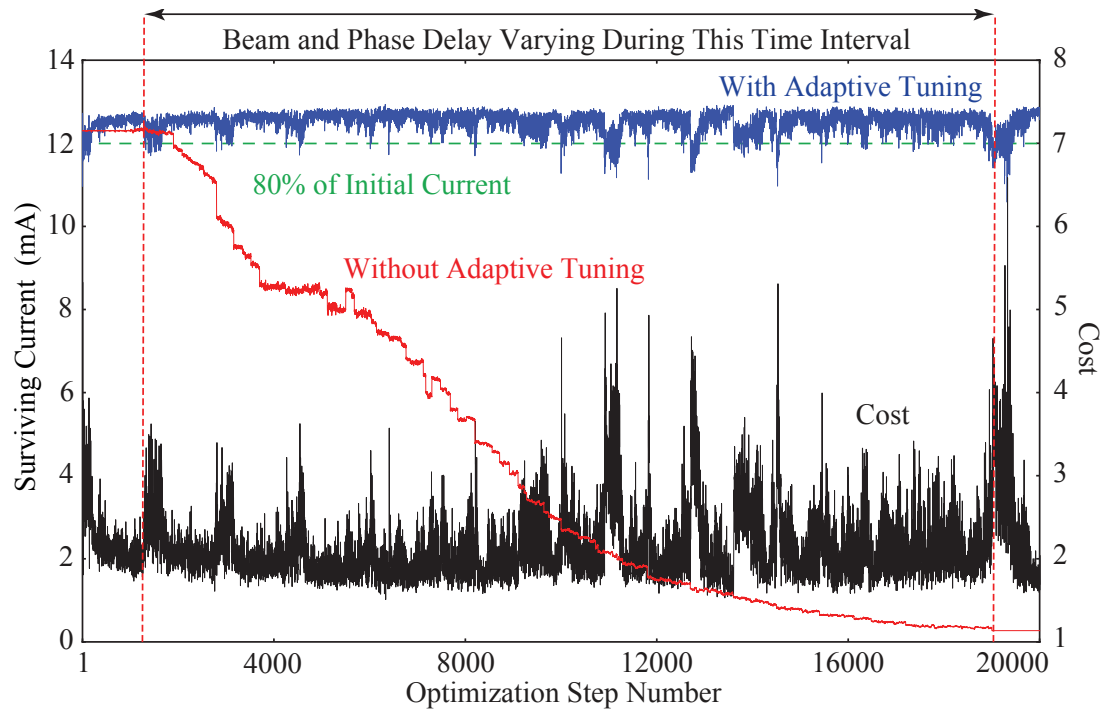


Figure 8.16: Surviving beam current at the end of the second DTL tank with and without adaptive RR tuning. The cost evolution during the tuning process is also shown.

Bibliography

- [1] R. Hajima, N. Taked, H. Ohashi, and M. Akiyama, Nucl. Instrum. Methods Phys. Res., Sect. A **318**, 822 (1992).
- [2] I. Bazarov and C. Sinclair, Phys. Rev. ST Accel. Beams **8**, 034202 (2005).
- [3] L. Emery, Global optimization of damping ring designs using a multi-objective evolutionary algorithm, in: PAC 2005, (2005).
- [4] M. Borland, V. Sajaev, L. Emery, A. Xiao, “Direct methods of optimization of storage ring dynamic and momentum aperture,” *Proc. PAC*, 2009.
- [5] L. Yang, D. Robin, F. Sannibale, C. Steier, and W. Wan, Nucl. Instrum. Methods Phys. Res., Sect. A **609**, 50, (2009).
- [6] A. Poklonskiy and D. Neuffer, Int. Journal. Modern. Phys., A, **24** 5 (2009).
- [7] W. Gao, L. Wang, and W. Li, Phys. Rev. ST Accel. Beams **14**, 094001 (2011).
- [8] R. Bartolini, M. Apollonio, and I.P.S. Martin, Phys. Rev. ST Accel. Beams **15**, 030701 (2012).
- [9] A. Hoffer, B. Terzic, M. Kramer, A. Zvezdin, V. Morozov, Y. Roblin, F. Lin, and C. Jarvis, Phys. Rev. ST Accel. Beams **16**, 010101 (2013).

- [10] M. Leblanc, “Sur l’electrication des chemins de fer au moyen de courants alternatifs de frequence elevee,” *Revue Generale de l’Electricite*, 1922.
- [11] W. H. Moase, C. Manzie, D. Nestic, and I.M.Y. Mareels. *Extremum seeking from 1922 to 2010*, in *29th Chinese Control Conference*, 14, 2010.
- [12] A. Scheinker, Ph.D. thesis, University of California, San Diego, November, 2012.
- [13] H. Khalil, *Nonlinear Systems*, Prentice Hall, NJ, 2002.
- [14] A. Scheinker, ‘Model Independent Beam Tuning,’ in: *IPAC 2013*, (2013).
- [15] A. Scheinker, X. Pang, and L. Rybarcyk, “Model-Independent Accelerator Tuning,” *Phys. Rev. ST Accel. Beams* **16**, 102803 (2013).
- [16] A. Scheinker and M. Krstic, “Extremum seeking with bounded update rates,” *Systems & Control Letters*, **63**, pp. 25-32, 2014.
- [17] M. Borland, “elegant: a flexible SDDS-compliant code for accelerator simulation,” *APS LS-287* (September 2000).
- [18] P.L. Kapitza, Dynamic stability of a pendulum when its point of suspension vibrates, *Soviet Phys. JETP* **21**, 588592 (1951).
- [19] X. Pang, L. Rybarcyk, and S. A. Baily, “High-performance beam simulator for the LANSCE linac,” *Proc. IPAC*, 2012.
- [20] X. Pang and L. Rybarcyk, “GPU accelerated online multiparticle beam dynamics simulator for ion linear particle accelerators,” submitted for publication to *Computer Physics Communications*.
- [21] J. Kurzweil and J. Jarnik, “Limit processes in ordinary differential equations,” *Journal of Applied Mathematics and Physics* vol. 38, March 1987, pp. 241-256.

-
- [22] H. J. Sussmann and W. Liu, “Limits of highly oscillatory controls and approximation of general paths by admissible trajectories.” *Proc. 30th IEEE CDC*, Brighton, UK, December, 1991.
- [23] H. J. Sussmann, “New differential geometric methods in nonholonomic path finding,” *Progress Systems and Control Theory*, pp. 365–384, 1992.
- [24] Y. Batygin, *Phys. Rev. E* **53**, 6020 (1998).
- [25] I. M. Kapchinsky, *Theory of Resonance Linear Accelerators* (Atomizdat, Moscow, 1966, Harwood, Chur. 1985).
- [26] Y. Batygin, *Phys. Rev. E* **53**, 5358 (1996).
- [27] Y. Batygin, *Phys. Rev. E* **53**, 5673 (1996).
- [28] Y. K. Batygin, A. Scheinker, “Nonlinear lattice for space-charge dominated beam transport with suppressed emittance growth,” *Proceedings of the 2012 International Particle Accelerator Conference*, New Orleans, 2012.
- [29] P.L. Walstrom, Preprint LA-UR-90-4090, (1990).